

Analysing eccentricity in gravitational waves

**AKSHAYA KRISHNA P
Reg. No. VPAVSPH003**

Supervisors:
**Dr. Tony Joseph
Syed Umair Husain Naqvi**

A dissertation submitted in fulfilment
of the requirement for the degree of
Bachelor of Physics



**Department of Physics
Government Victoria College, Palakkad 678001
University of Calicut, Kerala, India**

March, 2024

Analysing eccentricity in gravitational waves

Authored by:
AKSHAYA KRISHNA P

Supervisor:
Dr. Tony Joseph
Syed Umair Husain Naqvi
Department of Physics
Govt. Voctoria College, Palakkad 678001

CERTIFICATE OF EVALUATION

We approve the dissertation submitted by , in partial fulfilment of the requirements for the degree of Bachelor of Science in Physics, viva voce for the same was conducted on _____.

Examiner 1: _____

Examiner 2: _____



DEPARTMENT OF PHYSICS
GOVERNMENT VICTORIA COLLEGE
PALAKKAD, KERALA, INDIA, PIN 678001

CERTIFICATE

This is to certify that the thesis entitled **Analysing eccentricity in gravitational waves** is an authentic record of the research work carried out by **MS.AKSHAYA KRISHNA.P** in partial fulfillment of the requirements for the award of degree of Bachelor of Science in Physics (2021-24) under the University of Calicut. The work presented in this thesis has not been submitted for any other degree or diploma earlier.

11-03-2024
Palakkad

Dr Ambily Krishnan
Associate Professor and Head
Department of Physics
Government Victoria College
Palakkad 67800



**DEPARTMENT OF PHYSICS
GOVERNMENT VICTORIA COLLEGE
PALAKKAD, KERALA, INDIA, PIN 678001**

**CERTIFICATE
(Supervisor)**

This is to certify that the thesis entitled **Analysing eccentricity in gravitational waves** is an authentic record of the research work carried out by **AKSHAYA KRISHNA.P** under my supervision and guidance during 2021-24 in partial fulfilment of the requirements for the award of degree of Bachelor of Science in Physics under the University of Calicut .The work Presented in this thesis has not been submitted for any other degree or Diploma earlier.

Dr. Tony Joseph

Assistant Professor of Physics
Department of Physics
Government Victoria College
Palakkad 67800

11-03-2024
Palakkad

Acknowledgments

The work presented in this dissertation would not have been possible without the support of a number of a few individuals and I gratefully acknowledge all of them.

I owe my deepest gratitude to a great people who helped and supported me during this project work. My deepest thanks to Dr.Dr.Tony Joseph, Assistant Professor of Physics, Government Victoria College, Palakkad, and Mr. Syed Umair Husain Naqvi, PhD student in Department of Relativistic Astrophysics and Cosmology at Astronomical Observatory Jagiellonian University Krakow, Poland for supervising this work.

I express my deepest sense of gratitude to Dr Ambily Krishnan, Head of the Department of Physics, Government Victoria College, Palakkad for his wholehearted support during the course of this project.

I also extend my heartfelt thanks to my parents, friends and well wishers.

11-03-2024
Palakkad

AKSHAYA KRISHNA . P

Contents

Declaration	iii
Declaration	iv
Contents	v
1 Introduction and Theoretical Foundations	1
1.1 Evolution of Gravitational Theories	1
1.2 General Relativity Predictions	3
1.2.1 Gravitational waves	3
1.2.2 Precession of perihelion of mercury	4
1.2.3 Gravitational lensing	6
1.3 Gravitational waves	8
2 Gravitational Waves From Theory to Detection	12
2.1 Generation of gravitational Waves	12
2.2 Mathematical model of the binary system	14
2.3 Different types of sources	16
2.3.1 Cosmological sources	16
2.3.2 Relativistic Astrophysical Sources	18
2.3.3 Supernova explosions	19
2.3.4 Pulsar rotations	20
2.4 Detection of Gravitational Waves	21
3 Deep Dive into Inspiral Binary	24
3.1 Modeling Inspiral Waveforms	24
3.2 The post-Newtonian approximation	24

3.2.1 Effective one-body approach to general relativity	25
3.3 Post-Newtonian approximation for a binary system	25
3.3.1 Energy loss for circular orbits	28
3.3.2 Correction for elliptical orbits	28
3.4 Eccentric Binary Inspiral Evolution	29
3.5 Waveform Models	31
3.6 Results	35
3.6.1 Generating a Waveform Model using Python	39
3.7 Working code	39
4 PyCBC	48
4.1 The software environment setup	48
4.1.1 How can I get parameters?.....	49
4.2 Catalog of Binary Mergers	49
4.2.1 What binary mergers are in the catalog?	49
4.2.2 Transform Mass Parameters into the Detector Frame	50
4.3 Accessing LIGO/Virgo data around Specific Binary Merger in the Catalog	50
4.3.1 Getting Data from S5 / S6 / O1 and Getting Data from S5 / S6 / O1	52
4.4 Visualization of Data and Signal Processing	52
4.4.1 Viewing the raw LIGO data.....	52
4.4.2 Highpass and power spectral density (PSD) of the data ? and	53
4.4.3 Whitening the data and Visualizing excesses in the data with a Q-transform plot.	54
4.5 Generating Waveforms and Matched Filtering	56
4.5.1 calculate the power spectral density and signal model	57
4.6 signal-to-noise time series	58
4.7 Subtracting the signal from the data.	58
4.8 Results and conclusions...	59
4.8.1 mergers name in catalog	59

List of Figures

1.1 orbiting mass	4
1.2 mercury 1	5
1.3 mercury precession orbit	5
1.4 Curved spacetime	6
1.5 Deflection of light by the massive object	8
1.6 Deformations of rings	10
1.7 Plus and cross polarization of gravitational waves . .	10
2.1 A binary system consisting of point masses m_1 and M_2 , described in polar coordinates.	15
2.2 primordial gravitational waves signals.	17
2.3 Topological gravitational waves.	17
2.4 Binary source	18
2.5 Supernova expansion	19
2.6 Pulsar rotations	20
2.7 Gravitational waves from Pulsar rotations	21
2.8 LIGO Data source.	23
3.1	26
3.2	32
3.3	34
3.4 The figure for initial eccentricity = 0.1s and the orbital period = 0.3s	36
3.5 The figure for initial eccentricity = 0.2s and the orbital period = 0.3s	36
3.6 The figure for initial eccentricity = 0.2s and the orbital period = 0.3s	37

3.7 orbital period constant and eccentricity vary	37
3.8 Orbital and eccentricity constant mass ratio vary. as.1	38
3.9 mass ratio vary	38
3.10 Plus and the cross polarization for the initial eccentricity 0.1	40
3.11 Plus and the cross polarization for the initial eccentricity 0.1	41
3.12 With initial orbital period $P_0 = 01s$ and initial eccentricities e0=0.1 'This figure is taken from [Modeling and Measuring Eccentricity in Binary Black Hole Inspirals]'	41
3.13 With initial orbital period $P_0 = 01s$ and initial eccentricities e0=0.0001 'This figure is taken from [Modeling and Measuring Eccentricity in Binary Black Hole Inspirals]'	42
3.14 Program for the eccentricity and the orbital period .	42
3.15 Orbital period constant with varying eccentricity'1'	43
3.16 Orbital period constant with varying eccentricity'2'	43
3.17 Orbital period and the eccentricity constant with varying the masses'1'	44
3.18 Orbital period and the eccentricity constant with varying the masses'2'	45
3.19 Orbital period and the eccentricity constant with varying the masses ratio '1'	46
3.20 Orbital period and the eccentricity constant with varying the masses'2'	46
3.21 For the polarisation'1'	47
3.22 For the polarisation'2'	47
4.1 pip-comment-for-pycbc	48
4.2 Getting parameters	49
4.3 Mergers information	50
4.4 Transform Mass Parameters into the Detector Frame	51
4.5 Time series data for GW150914	51
4.6 Getting Data from S5 / S6 / O1	52
4.7 Reading-gravitational-wave-frame	52
4.8 Viewing-the-raw-ligo-data	53
4.9 Applying highpass filter to data	54
4.10 PSD	54

LIST OF FIGURES

x

4.11 whiltening the data	55
4.12 Coherent signal that matches in phase for a few cycles	55
4.13 Q-transform	55
4.14 Generating waveform	56
4.15 power spectral density	57
4.16 signal model	58
4.17 Aligning and Subtracting the Proposed Signal	58
4.18 Subtracting the signal from the data	59
4.19 Duration32.0s Start1126259447 End126259479	60
4.20 Data for this demonstration	60
4.21 'H1', 'L1'	61
4.22 Zoomed to 0.5s	61
4.23 highpass frequency	62
4.24 psd is a FrequencySeries	62
4.25 Whiten the data	63
4.26 Apply a highpass filter (at 30 Hz) followed by an lowpass filter (at 250 Hz)	63
4.27 Apply a highpass filter (at 30 Hz) followed by an lowpass filter (at 250 Hz) to tighter	63
4.28 specially align the L1 data	64
4.29 Visualizing excesses in the data with a Q-transform p	64
4.30 Visualizing excesses in the data with a Q-transform p	64
4.31 TEST-STRAIN	65
4.32 Generating waveform	65
4.33 Waveform zoomed to 0.01s	66
4.34 Waveform change with the mass of the binary	66
4.35 Changing the distance of the waveform	67
4.36 Remove the low frequency content and downsample the data to 2048Hz	67
4.37 Remove 2 seconds of data from both the beginning a end	68
4.38 Power spectral density	68
4.39 Our signal model and matched filtering involves laying the potential signal over our data and integrating	69
4.40 Calculating the signal-to-noise time series	69
4.41 Visualize the overlap between the signal and data	69

LIST OF FIGURES

xi

4.42 Subtracting the signal from the data	70
4.43 Subtracting the signal from the data	70

List of Tables

Abstract

Chapter 1

Introduction and Theoretical Foundations

1.1 Evolution of Gravitational Theories

The development of Newtonian gravity is a major contribution in early science. Sir Isaac Newton formulated his theory of gravity in the late 17th century, building on the work of earlier scientists such as Galileo Galilei and Johannes Kepler. Newton's breakthrough came when he realized that the same force that causes objects to fall to the ground (gravity) is responsible for keeping the Moon in its orbit around the Earth. He recognized that the force of gravity must extend throughout the universe and that it could explain the motion of the planets and other celestial bodies. Newton's law of universal gravitation, which describes the force between two objects with mass, was published in his landmark work, *Philosophiæ Naturalis Principia Mathematica*, in 1687. The theory revolutionized our understanding of the universe and provided a foundation for later developments in physics and astronomy. He provide the equation as :

$$F = \frac{GMm}{r^2} \quad (1.1)$$

Where G is the gravitational constant , M and m are the masses of objects and the distance between the objects scientific knowledge advanced,

certain phenomena could not be adequately explained by Newtonian gravity. For example, the anomalous precession of the orbit of Mercury and the deflection of light passing near massive objects like the Sun etc. At that time Albert Einstein introduced his theory of Special Relativity, which revolutionized our understanding of space and time, showing that they are intertwined in what he called space-time. He introduced the new concept of the mass-energy relation

$$E = Mc^2 \quad (1.2)$$

Though Special Relativity showed that the laws of physics are the same for all observers in uniform motion, and the speed of light is constant in all inertial frames of reference. Building upon the foundations of Special Relativity, Einstein developed his theory of General Relativity in 1915, which provides a new description of gravity. In this theory, gravity is not seen as a force; instead, it is described as the curvature of spacetime caused by the mass and energy. In this framework, all massive objects move like a curved path. This theory successfully explains the observed anomalies in mercury's orbit and predicts phenomena like gravitational time dilation and gravitational waves. General relativity gives a relationship between curvature and the density of mass and energy in space, which can be written symbolically as

$$G^{\mu\nu} = R^{\mu\nu} - \frac{1}{2}g_{\mu\nu} = \frac{8\pi G}{c^4} \quad (1.3)$$

This expression incorporates gravitation (Newton's constant G) and special relativity (the speed of light c). If no matter or energy is present, the right-hand side is zero; as a result, the curvature is zero and space is flat. In the limit of classical kinematics and in the limit of weak gravitational fields ($G \rightarrow 0$), space is nearly flat and we can safely use the Newtonian gravitational theory. If we increase its radius to a sufficiently large value, the geometry is approximately Euclidean, as classical kinematics can

be regarded as the limiting case of special relativity (for low speeds), so can classical gravitation be regarded as the limiting case of general relativity (for weak fields). In calculating the orbit of an Earth satellite or the trajectory of a space probe to Mars, Newton's theory gives entirely satisfactory results. Close to the Sun and to compact or massive stars, the curving of space can lead to observable effects.

1.2 General Relativity Predictions

General Relativity (GR) has made several successful predictions that have been confirmed through experimental observations. These successful predictions have solidified the validity of Einstein's GR and demonstrated its accuracy in describing the behavior of gravity and spacetime. Here are some notable predictions of GR:

1.2.1 Gravitational waves

Just as an accelerated charge emits electromagnetic radiation that travels with the speed of light, an accelerated mass emits gravitational radiation that also travels with the speed of light. In effect, gravitational waves are ripples that travel through spacetime. Waves produced by such motions as the planets around the Sun are exceedingly weak and beyond any hope of detection. Cataclysmic events in the universe, such as supernova explosions, and highly accelerated systems, such as compact binary objects, may produce observable gravitational waves. Detection of these waves would provide another important confirmation of general relativity theory. In analogy with the effect of a passing electromagnetic wave on a charged particle, a passing gravitational wave could be detected by its effect on matter. Several antennas have been built to search for gravity waves, but no conclusive experimental evidence has yet been obtained.

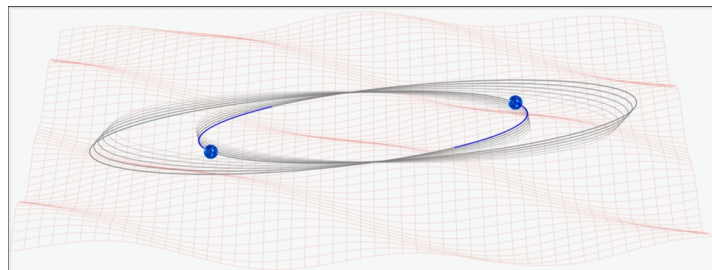
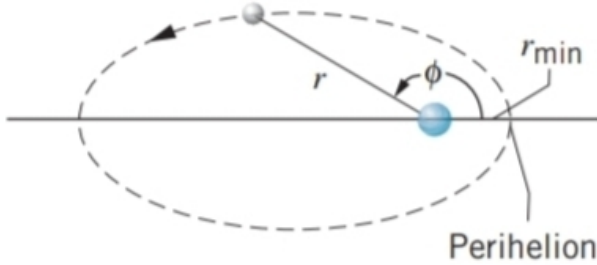
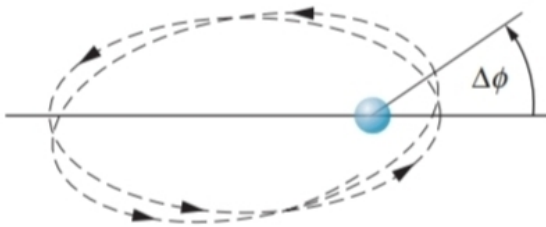


Figure 1.1 orbiting mass

has come from the observations of the change in the ~~perihelion~~ of a binary pulsar (see next section). Interferometric techniques are being used to build new detectors to search for gravitational ~~waves~~. The Laser Interferometer Gravitational-wave Observatory (LIGO), which began operation in 2001, consists of two installations (located in the states of Washington and Louisiana) whose interferometer arms are 4 km ~~in length~~. A passing gravitational wave would cause a ~~small~~ change in the length of one arm relative to the other, which would be detected through a change in the fringe pattern similar to that of the Michelson interferometer[2].

1.2.2 Precession of perihelion of mercury

Mercury perihelion advance is a phenomenon that puzzled the astronomers for centuries. Previous studies suggested that this is due to the influence of the sun. However, there is still much that is not known about the exact mechanism. This gap is filled by investigating the role of the general theory of relativity. Relativity plays a significant role in the mercury's perihelion advance, which explained that this is due to the curvature of the spacetime. Consider a simple planetary system, shown in the figure(1.2) consisting of a single planet in orbit about a star of mass M such as the Sun. According to Newtonian gravitation, the orbit is a perfect ellipse with the star at one focus [2]. The equation of the ellipse is

**Figure 1.2**mercury**Figure 1.3**mercury precession orbit

$$r = r_{min} \frac{1 + e}{1 + e \cos \varphi} \quad (1.4)$$

where r_{min} is the minimum distance between planet and star and e is the eccentricity of the orbit (the degree to which the ellipse is noncircular; $e = 0$ for a circle). When $r = r_{min}$, the planet is said to be at perihelion; this occurs regularly, at exactly the same point in space, whenever $2\pi, 4\pi, \dots$. According to general relativity, the orbit is not quite a closed ellipse; the curved spacetime near the star causes the perihelion direction to precess somewhat, as shown in Figure 1.3. After completing one orbit, the planet returns to r_{min} , but at a slightly different angle. The difference can be computed from general relativity, according to which the orbit is $r =$

$$r = r_{min} \frac{1 + e}{1 + e \cos \varphi - \delta \varphi} \quad (1.5)$$

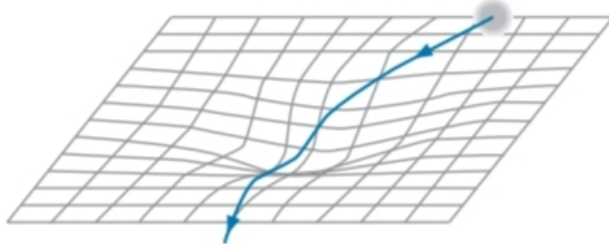


Figure 1.4 Curved spacetime

$$\delta\phi = \frac{6\pi GM}{c^2 r_{min}(1 + e)} \quad (1.6)$$

The measured values are in agreement with the predictions of general relativity[2].

1.2.3 Gravitational lensing

Gravitational lensing is another phenomenon based on the general theory of relativity. According to the general theory which predicts that massive objects, such as galaxies or galaxy clusters, can distort the fabric of spacetime around them. This distortion then affects the path of light traveling through this curved spacetime. When light passes close to a massive object, its path is bent due to the curvature of spacetime, shown in the figure(1.4).

This bending of light is what causes the phenomenon of gravitational lensing. The light rays from a distant source are deflected as they pass through the gravitational field of the massive object, resulting in a change in their direction. The general theory of relativity provides us with the mathematical framework to calculate and predict the extent of this bending of light as

$$R_{mv} - \frac{1}{2}Rg_v = \frac{8\pi G}{c^4}T_{mv} \quad (1.7)$$

Here $R_{\mu\nu}$ is the Ricci curvature tensor, R is the scalar curvature, the metric tensor, T is the stress-energy tensor, G is the gravitational constant, and c is the speed of light. This allows us to understand and describe the formation of multiple images, Einstein rings, and other observable effects of gravitational lensing. Gravitational lensing has been observed and confirmed through numerous astronomical observations, providing strong evidence for the validity of Einstein's general theory of relativity. Relativity continues to be an important field of study in astrophysics, contributing to our understanding of the cosmos and the nature of gravity.

Deflection of straight line Consider another case the Deflection of straight line. The deflection of light by a gravitational field is another prediction of general relativity, which states that light will follow a curved path when passing through star gravity. The deflection angle can be calculated using the equation

$$\theta = \frac{2GM}{Rc^2} \quad (1.8)$$

Where M is the mass of star, R is the radius. Consider the deflection of the light by the sun by an angle θ shown in the figure (1.5).

Substituting the numbers gives 0.87 as the prediction. Special relativity and Newtonian gravitation gives a different view. Spacetime in the vicinity of the Sun is curved, and the light beam is simply following the most direct path along the curved spacetime. According to general relativity, the expected deflection is 1.74°, exactly twice the value predicted by the Newtonian formula[2].

Measuring this effect requires the observation of a beam of light, such as from a star that passes near the edge of the Sun. Light near the Sun can be observed only during a total solar eclipse in 1919, just a few years after Einstein completed his general theory, two expeditions of British astronomers traveled to Africa and to South America to observe the solar

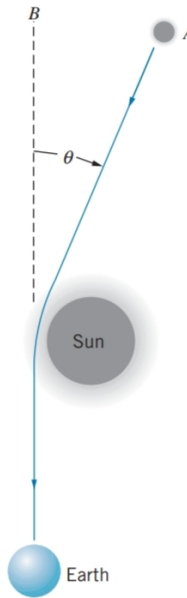


Figure 1.5 Deflection of light by the massive object

eclipse and to measure the apparent changes in positions of stars whose light grazed the Sun. Their results for the deflection angles, 1.98 ± 0.18 and 1.69 ± 0.45 , gave strong support for the new general theory. years since those early results, this experiment has been repeated at nearly every total solar eclipse, and the overall agreement with general relativity. Radio emission from quasars has also been used to confirm this effect, which agreement with general relativity[2].

1.3 Gravitational waves

The gravitational waves are the ripples in the space time we early see that in the above sectionThen just like the electromagnetic waves the gravitational waves have two polarization and they are easily absorbed and scattered by the medium of the propagation, affected by the intervening medium due to the weak interaction of gravity.Einstein's geometry

connects the spacetime with the matter distribution in the following way,

$$R_{\mu\nu} - \frac{1}{2}g_{\mu\nu}R = \frac{8\pi G}{c^4}T_{\mu\nu} \quad (1.9)$$

Where $R_{\mu\nu}$ is called the Ricci tensor, R is Ricci scalar and $T_{\mu\nu}$ is called energy momentum tensor characterizing the gravitational constant and the speed of light is represented by G . The space time represented by the metric $g_{\mu\nu}$ which is given as $ds^2 = g_{\mu\nu}X^\mu X^\nu$ where $\mu, \nu = 0, 1, 2, 3$. and x are the corresponding coordinates. To understand this equation let's assume the space time is nearly flat then studied as the expansion around flat spacetime. This method is called the linearized gravity approximation. In this case we write spacetime metric as $g_{\mu\nu} + h_{\mu\nu}$, Where the $\eta_{\mu\nu}$ is the flat spacetime metric and $h_{\mu\nu}$ is the small perturbation to it. Linearized theory has a redundant gauge freedom which is invariance of the theory under the coordinate transformations $x^\mu \rightarrow x^\mu + \zeta^\mu$. Then the equation (1.9) reduced into ,

$$2h^\mu + \eta_{\mu\nu}\partial^\rho\partial^\sigma h_{\rho\sigma} = \frac{-16\pi G}{c^4}T_{\mu\nu} \quad (1.10)$$

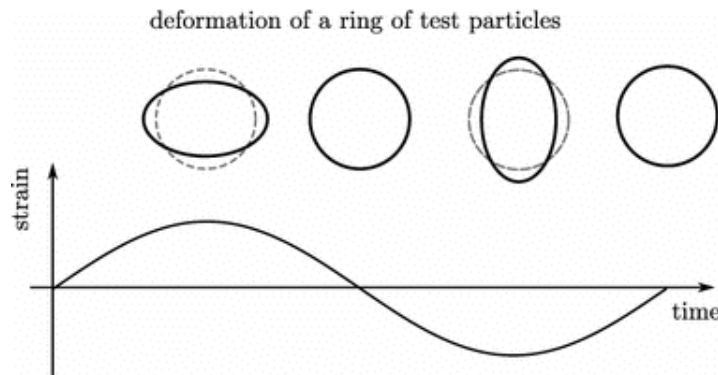
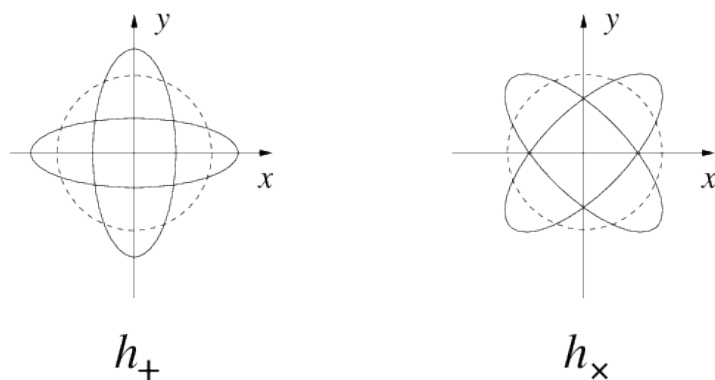
The same gauge freedom can be used to choose the Lorentz gauge , which reduces to

$$2h_{\mu\nu} = \frac{-16\pi G}{c^4}T_{\mu\nu} \quad (1.11)$$

After solving the equation (1.11) for a slowly moving source the components can be neglected, then obtain the solution as

$$h_{ij}^{TT}(t, x) = \frac{2G}{rc^4}Q_{ij}(t - r/c) \quad (1.12)$$

Where the $t(-r/c)$ represent the retarded time , Q the quadrupole moment of the source and r is the distance to the source. The equation (1.12)

**Figure 1.6** Deformations of rings**Figure 1.7** Plus and cross polarization of gravitational waves

is called the quadrupole form~~balance~~ any source with non-vanishing second time derivative of quadrupole moment can emit gravitational waves and the amplitude is always inversely related to the distance to the source r , shown in figure(1.7) Most importantly, the solution given in equation (1.12) has only two degrees of freedom as a consequence of symmetries of Einstein's equations which we imposed through this particular gauge choice and the gravitational wave strain satisfies the conditions[2].

This implies that we finally obtain a transverse plane wave solution with two independent components correspond to two polarization states of the wave the plus and the cross polarization shown in the figure (1.8).

When a gravitational wave passes orthogonally through a ring of test masses, the relative separation between the test masses changes as an effect

of the waveThis will change the shape of the ring depending upon the polarisation state of the gravitational ~~Wave~~^{Waves}property of gravitational waves is used in interferometric gravitational ~~wave~~^{wave}detectors As in the case of electromagnetic theory where the Poynting flux is proportional to the square of the first time derivative of the vector potential, here the GW flux is proportional to the first time derivative of the amplitude of the GW given in equation (1.11)that is the GW flux is proportional Q_p . In this approximation we also get the luminosity of gravitational ~~wave~~^{wave} . quadrupole moment in equation (1.12) can be expanded at the leading order as an integral of the mass density as ,

$$Q = \int d^3x T_{00}(t, x) X_i X_j \quad (1.13)$$

Where the Q as the quadrupole moment, T_{00} as mass density, X_i is time components of the stress x^i and dx_j are the corresponding coordinates axis.From the above equations we conclude that the Gravitational waves will be detectable only from a source which is highly relativistic and whose compactness is close to the maximum value[2].

Chapter 2

Gravitational Waves From Theory to Detection

2.1 Generation of gravitational Waves

In this section we discuss how gravitational waves are emitted in the first place. The discussion mirrors the one found in Misner, Thorne and Wheeler [9]. In order to estimate how much gravitational radiation a binary system emits we can use the similarities between the linearised theory of gravity and Maxwell's theory of electromagnetism, known as gravitoelectromagnetism, to perform a multiple expansion of the stress energy tensor $T^{\mu\nu}$ to identify the leading term.

In electromagnetism the electric dipole term is the leading one. The power output, or luminosity (denoted L), from an electric-dipole configuration is in geometrical units

$$L_{ed} = \frac{2}{3} p \cdot \ddot{p} \quad (2.1)$$

where \ddot{p} is the second time derivative of the dipole moment p [9]. The gravitational analogue of the electric dipole moment is the mass dipole moment d given by

$$d = \sum_i m_i x_i \quad (2.2)$$

But no gravitational radiation can then be generated from a mass dipole.

For

$$d = \sum_i m_i x_i = p \quad (2.3)$$

is just the total momentum of the system (not to be confused with the electric dipole moment denoted with the same symbol), so the second derivative d must vanish as momentum is a conserved quantity.

The second strongest source of electromagnetic radiation is the magnetic dipole. Magnetic dipole radiation is generated by the second derivative of the magnetic moment. The gravitational analogue to the magnetic dipole moment is the angular momentum

$$J = \sum_i x_i \times (m v_i) \quad (2.4)$$

which like momentum is a constant of motion. Thus there can be no radiation from this term either. We therefore see that there can be no gravitational radiation whatsoever from dipole sources in the multipole expansion are the quadrupole terms. The luminosity of an electromagnetic quadrupole source is

$$L_{eq} = \frac{1}{20} Q_{ij}^{ij} Q_{jk}^{jk}, \quad (2.5)$$

where

$$Q_{jk} = \sum_i q x_{ij} x_{ik} - \frac{1}{3} \delta_{jk} X_i^2 \quad (2.6)$$

is the electromagnetic quadrupole moment. The gravitational analogue to this is the mass quadrupole moment tensor defined as

$$I_{jk} = \sum_i x_j x_k - \frac{1}{3} \delta_{jk} X_i^2 \quad (2.7)$$

and we can use this to obtain the power output, or luminosity, as

$$L_{mq} = \frac{I}{5} \quad (2.8)$$

This is the first nonzero term, which will dominate in the SM approximation, and we will use this later on in our calculations for binary systems. that this expression is given in geometrical units, if we want to compare our result with the order of magnitudes in everyday life it would be neat to be able to convert our result to SI units. We can use the expression

$$L(SI) = \frac{c^5}{G} L(\text{geometrised}) \quad (2.9)$$

to convert between these units[3] .

2.2 Mathematical model of the binary system

Consider the following model of a general binary system. Two masses M and m be in elliptical orbit about one another in the xy -plane, see figure(2.1) . The reduced mass of the binary system is

$$\mu = \frac{Mm}{M + m} \quad (2.10)$$

If we use polar coordinates with the origin placed in the center of mass, the positions of the two masses are $(\mathbf{r}_1(t), \theta)$ and $(\mathbf{r}_2, \theta + \pi)$ both depending on time . The total separation is $\mathbf{d}(t) = \mathbf{r}_1(t) + \mathbf{r}_2(t)$, and by the definition of center of mass it must hold that $\mu \mathbf{d}(t) = m \mathbf{r}_1 + M \mathbf{r}_2$. solving for \mathbf{r}_1 and \mathbf{r}_2 gives

$$\mathbf{r}_1 = \frac{M}{M + m} \mathbf{d}, \mathbf{r}_2 = \frac{m}{M + m} \mathbf{d} \quad (2.11)$$

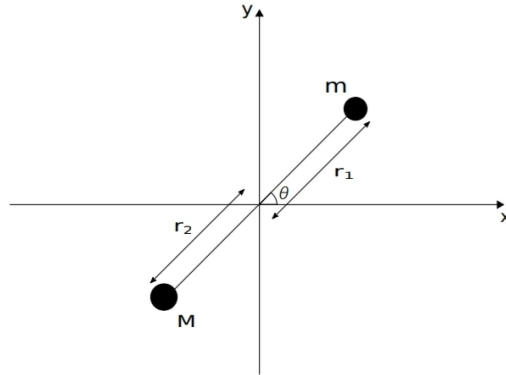


Figure 2.1A A binary system consisting of point masses m and M , described in polar coordinates.

We can now use Newton's extension of Kepler's laws of planetary motions, which gives us

$$d(t) = \frac{a(1 - \varepsilon^2)}{1 + \varepsilon \cos \theta(t)} \quad (2.12)$$

where ε is the eccentricity of the elliptical path, a is the semi-major axis of the ellipse, and d is defined as in figure 2.1. Kepler's laws also give us the expression for angular velocity ω as

$$\omega = \dot{\theta} = \frac{a(M + m)(1 - \varepsilon^2)^{3/2}}{d(t)^2} \quad (2.13)$$

From the Equation [3] allows us to calculate the quadrupole tensor for the system as [3.3.17].

It is in principle straightforward to calculate the derivatives and use Equation [3.3.18] to get the power radiated by the system. When we are interested in the order of magnitude of the radiation in SI units we can use Equation [3.3.15].

2.3 Different types of sources

The sources of gravitational waves can be broadly categorized into two main types: cosmological and relativistic astrophysical sources.

2.3.1 Cosmological sources

Primordial gravitational waves

Primordial gravitational waves are generated during the early stages of the universe, specifically during cosmic inflation, which is a rapid expansion thought to have occurred shortly after the Big Bang. These gravitational waves are a consequence of quantum fluctuations in the fabric of spacetime during inflation. The detection of primordial gravitational waves can provide valuable insights into the physics of the early universe, including the nature of inflation and the fundamental properties of space-time. Advanced gravitational wave detectors, such as the BICEP/Keck and the upcoming Lite BIRD mission, are specifically designed to search for the faint signals of primordial gravitational waves. The confirmation of primordial gravitational waves would be a significant milestone in our understanding of the universe's origins and evolution.

Phase Transitions gravitational waves

Phase transitions in the early universe, such as the transition from a symmetric phase to a broken symmetry phase, can generate gravitational waves. During these phase transitions, rapid changes in the energy density and the dynamics of the fields can lead to the production of gravitational waves. The detection of gravitational waves from phase transitions can provide insights into the fundamental physics of the early universe, including the properties of particle physics beyond the Standard Model.

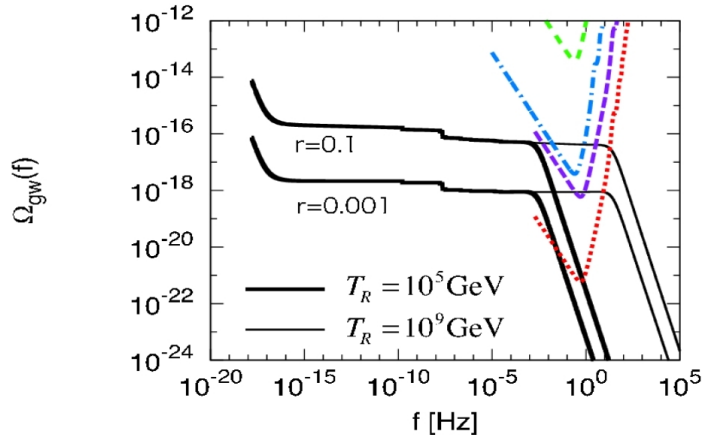


Figure 2.2 primordial gravitational waves signals

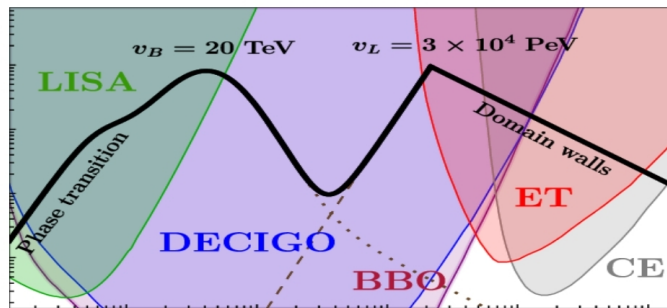


Figure 2.3 Topological gravitational waves

gravitational wave detectors such as LIGO and future missions like the Einstein Telescope, are designed to search for the signals of gravitational waves from phase transitions. The observation of gravitational waves from phase transitions would offer valuable information about the evolution of the universe and the fundamental forces at play during its early stages.

Topological Defects gravitational waves

Topological defects are theoretical entities that can form during phase transitions in the early universe, such as the transition from a symmetric phase to a broken symmetry phase. Examples of topological defects include cosmic strings, monopoles, and domain walls, which are formed due to

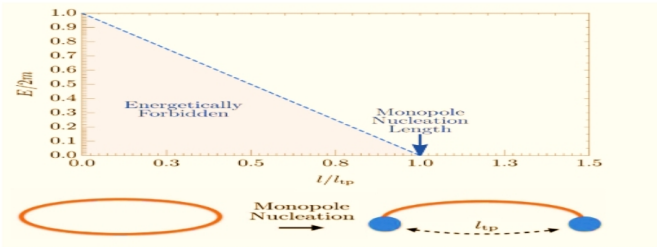


Figure 2.4 Binary source

the breaking of symmetries in the early universe. These defects can have significant effects on the evolution of the universe, including the generation of gravitational waves. Gravitational waves produced by topological defects have distinct signatures that can be detected by advanced gravitational wave detectors such as LIGO and future missions like the Einstein Telescope. The detection of gravitational waves from topological defects would provide valuable insights into the physics of the early universe and the fundamental forces at play during phase transitions. While there have been no direct observations of topological defects or their associated gravitational waves, ongoing research and advancements in gravitational wave detection offer promising prospects for their detection in the future.

2.3.2 Relativistic Astrophysical Sources

In this category also they are different types are Binary inspirals , Supernova explosions and Pulsar rotations gravitational waves .

Binary inspirals

Binary inspirals, such as merging black holes or neutron stars, are one of the primary sources of gravitational waves. As compact objects like black holes or neutron stars orbit each other, they emit gravitational waves that carry away energy and angular momentum. Advanced gravitational wave

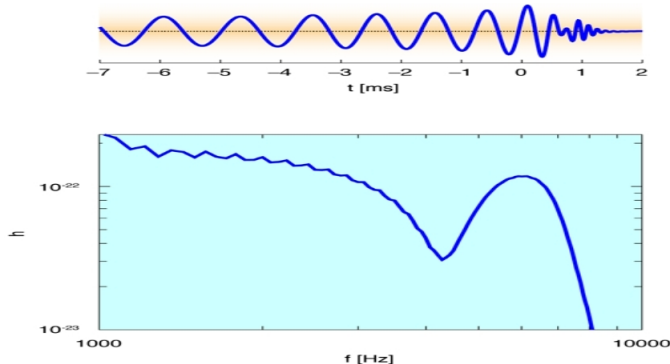


Figure 2.5Supernova expansion

detectors like LIGO and future missions like the Einstein Telescope are designed to detect and study gravitational waves from binary inspirals . The detection of binary inspirals provides valuable insights into the nature of compact objects, their masses, spins, and the dynamics of their mergers . Studying binary inspirals can also help test the predictions of general relativity and explore the properties of spacetime in extreme conditions . The observation of binary inspirals has already led to significant discoveries, such as the first direct detection of gravitational waves from merging black holes .

2.3.3 Supernova explosions

Supernova explosions are one of the main sources of gravitational waves in the universeWhen a massive star undergoes a supernova explosion, it releases an enormous amount of energy and creates a shockwave that propagates through spaceThis shockwave can generate gravitational waves, which are ripples in the fabric of spacetime, as predicted by general relativity .Gravitational wave detectors like LIGO and future missions like the Einstein Telescope are designed to detect and study gravitational waves from supernova explosionsDetecting gravitational waves from supernova explosions can provide valuable insights into the physics of stellar collapse,

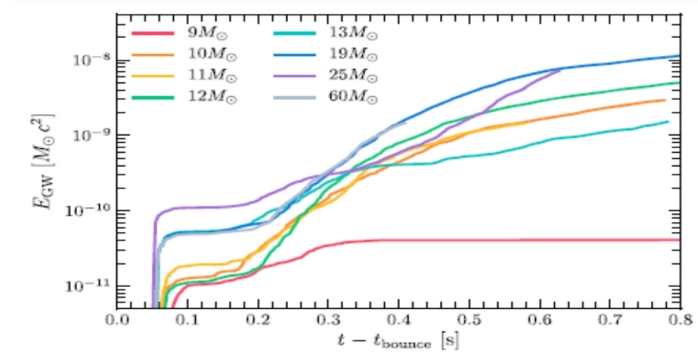


Figure 2.6Pulsar rotations

the formation of neutron stars and black holes, and the dynamics of these explosive events. Studying gravitational waves from supernova explosions can also help us understand the nucleosynthesis processes that occur during these events and contribute to the enrichment of the universe with heavy elements.

2.3.4 Pulsar rotations

Pulsar rotations can also generate gravitational waves, although they are not as strong as those from binary inspirals or supernova explosions. Pulsars are considered as the rotating neutron stars that emit beams of electromagnetic radiation. They are highly magnetized. As pulsars rotate, they can emit gravitational waves due to their asymmetrical mass distribution and the changing quadrupole moment of their rotating magnetic fields. Gravitational wave detectors like LIGO and future missions like the Einstein Telescope are designed to detect and study gravitational waves from pulsar rotations. Studying gravitational waves from pulsar rotations can provide insights into the properties of neutron stars, their internal structure, and the behavior of matter under extreme conditions. Detecting gravitational waves from pulsar rotations can also help test the predictions of general relativity and provide further evidence for the existence of gravitational

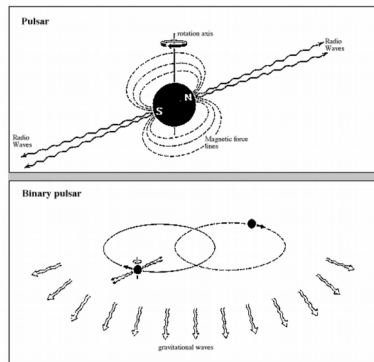


Figure 2.7 Gravitational waves from Pulsar rotations

waves .

2.4 Detection of Gravitational Waves

Scientists have been attempting to detect gravitational waves for many years. Early attempts to detect gravitational waves were made using large-scale bar detectors, such as the Weber bar detector, in the 1960s and 1970s. However, these early detectors were not sensitive enough to detect the weak signals from gravitational waves. In the 1980s, the development of laser interferometry opened up new possibilities for detecting gravitational waves. The Laser Interferometer Gravitational-Wave Observatory (LIGO) was established in the United States, and similar projects were initiated in other countries. The first generation of LIGO detectors operated from 2002 to 2010 but did not detect any gravitational waves. However, they provided valuable insights and paved the way for the more sensitive second-generation detectors. In 2015, the Advanced LIGO detectors, with improved sensitivity, began their first observing run and made the historic detection of gravitational waves in 2016. This detection confirmed the existence of gravitational waves and opened up a new era of gravitational wave astronomy. The first direct evidence of the existence of gravitational waves and the

observation of the merger of a binary black hole system was made by the LIGO and Virgo collaborations in 2016. The detections named GW151226 and GW170104 are also consistent with the merger of two black holes. Hulse and Taylor binary neutron star system provided the first indirect astrophysical evidence of the existence of gravitational waves. The size of the binary orbit decreases and the components move faster, leading to the emission of gravitational waves with increasing amplitude and frequency. This stage is known as the chirp signal.

Challenges of Detection of Gravitational Waves

The detection of gravitational waves posed several challenges for scientists. Gravitational waves are extremely weak and require highly sensitive instruments to detect them. The LIGO and Virgo collaborations developed advanced detectors that were able to measure tiny changes in the length of their arms caused by passing gravitational waves. Another challenge was distinguishing gravitational wave signals from background noise. Extensive data analysis techniques were employed to filter out noise and identify genuine gravitational wave signals. Overall, the detection of gravitational waves required the development of sophisticated instruments, advanced data analysis techniques, and a deep understanding of the expected signals and their characteristics.

The breakthrough of LIGO (Laser Interferometer Gravitational-Wave Observatory) and Virgo collaborations came on February 11, 2016, with the announcement of the first observation of gravitational waves. This discovery provided direct evidence for the existence of gravitational waves and marked the first observation of the merger of binary black hole systems. The detected gravitational wave signal, named GW150914, was produced by the spiral and merger of a binary black hole system. In accordance with the predictions of general relativity, the LIGO and Virgo collaborations played

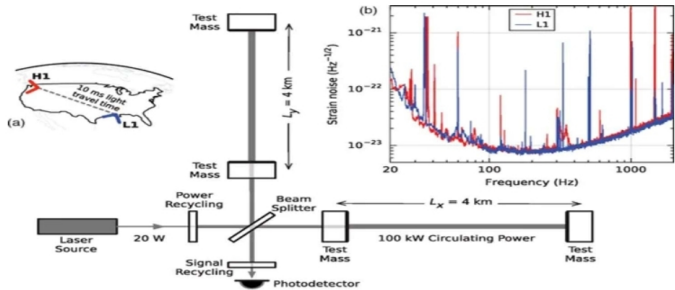


Figure 2.8LIGO Data source

a crucial role in this breakthrough, with LIGO being the primary observatory and Virgo providing additional support and ~~data~~detection opened up a new era of gravitational wave astronomy, allowing scientists to study the universe in a completely different way and providing insights into the nature of black holes, neutron stars, and other astrophysical phenomena.

Detection Principle

LIGO (Laser Interferometer Gravitational-Wave Observatory) and Virgo use the principle of interferometry, specifically Michelson interferometry, to detect gravitational waves .

LIGO consists of two L-shaped interferometers with perpendicular arms, while Virgo is a similar interferometer located in Italy. beams are split and sent down the arms of the interferometers,they bounce off mirrors and return to the point of origin. Gravitational waves passing through the interferometers cause tiny changes in the lengths of the arms, resulting in a phase shift in the laser beams. By comparing the phase shifts of the laser beams, LIGO and Virgo can detect and measure gravitational waves. The interference pattern created by the recombined beams provides information about the source of the waves. The detection of GW150914, the first observed gravitational wave, was made possible by the precise measurements of LIGO and Virgo and the subsequent analysis of the data.

Chapter 3

Deep Dive into Inspiral Binary

3.1 Modeling Inspiral Waveforms

The parameterized post-Einsteinian framework modifies inspiral waveform models to incorporate effects beyond General Relativity. Extending the existing model into the merger-ringdown regime, modification introduced here adds a single degree of freedom that corresponds to a change in the binary coalescence time. Other merger properties remain as predicted by GR. We discuss parameter estimation with this model, and how it can be used to extract information from beyond-GR waveforms.

3.2 The post-Newtonian approximation

The post-Newtonian approximation is an expansion in $v/c \sim L/\lambda \sim L/c/P$ where v , $L\lambda$ and P are the characteristic velocity, size, wavelength and period respectively. Largely it is an expansion in v/c and is also called slow motion expansion. It uses Newtonian concepts like absolute space, with an Euclidean metric and absolute time. Newtonian techniques and in this viewpoint, Einstein's theory provides small numerical corrections to Newtonian theory. The equations in this scheme are a hierarchy of Poisson equations which are solved by instantaneous potentials.

3.2.1 Effective one-body approach to general relativistic

We map the general relativistic two-body problem onto that of a test particle moving in an effective external metric. This effective-one-body approach defines in a non-perturbative manner the late dynamical evolution of a coalescing binary system of compact objects. The transition from the adiabatic inspiral, driven by gravitational radiation damping, to an unstable plunge induced by strong spacetime curvature is predicted to occur for orbits more tightly bound than the innermost stable circular orbit in a Schwarzschild metric of mass $M = m_1 + m_2$. The binding energy, angular momentum and orbital frequency of the innermost stable circular orbit for the time-symmetric two-body problem are determined as a function of the mass ratio.

3.3 Post-Newtonian approximation for a binary system

Coalescence of two black holes is the more intensive source of GW generations. The Newtonian order approximation for a binary inspiral signal is represented by two masses, m_1 and m_2 , separated by a distance R (assuming a circular orbit) and orbiting the reduced mass of the system $\mu = \frac{m_1 m_2}{m_1 + m_2}$. An orbital plane intersects the y -axis, making an angle ι with the z -axis shown in figure(3.1). Parametrizing the position for a circular orbit $\mathbf{r} = \mu \frac{1 + e \cos \omega t}{m_1 + m_2} \mathbf{e}(t)$ and $\mathbf{X} = R \frac{\mu}{m_2} \mathbf{e}(t)$ where $\mathbf{e}(t) = [\cos \omega t, \sin(\omega t), \sin(\omega t) \sin(\iota)]$ [17]. The equation for the spiral tensors are

$$h_x = \frac{1}{r c^4} (M_{11} - M_{22}) \quad (3.1)$$

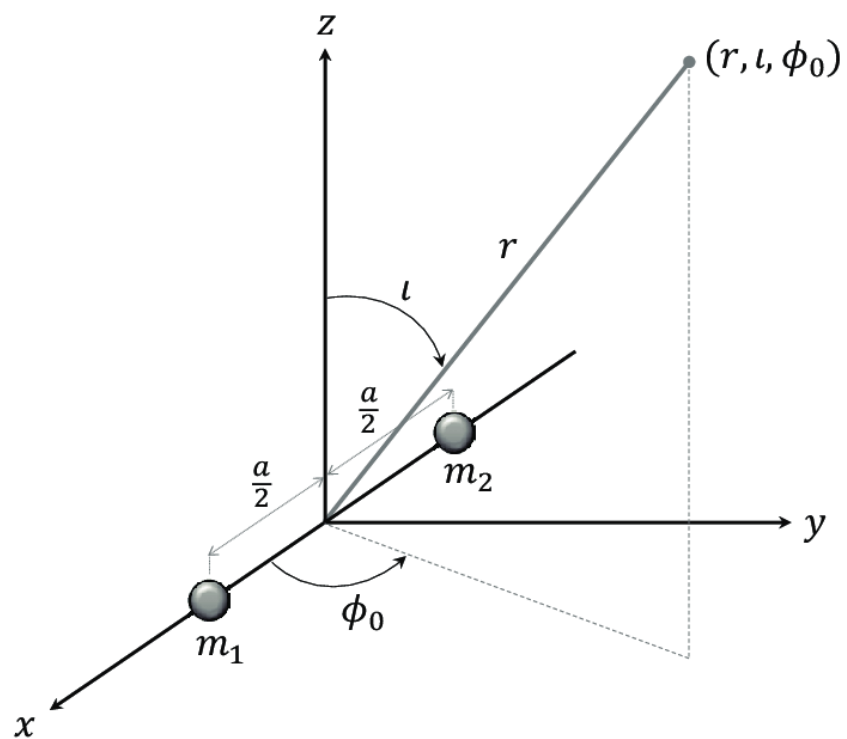


Figure 3.1

$$h_+ = \frac{2G}{rC^4} M_{12}^{\ddot{\cdot}} \quad (3.2)$$

The componentes of the spatial tensor [5.Bq8,5.3.9] are

$$M_{11} = R\mu \cos^2(\omega t) \quad (3.3)$$

$$M_{22} = R^2 \mu \sin^2(\omega t) \cos^2(i) \quad (3.4)$$

$$M_{12} = R^2 \mu \cos(\omega t) \sin(\omega t) \cos^2(\phi) \quad (3.5)$$

Introducing the spatial tensor in the polarization tensor, we obtain

$$h_+ = \frac{4(GM)}{rC^2} \left(\frac{\pi f(t)}{c} \right)^{2/3} \frac{1 + \cos}{2} \cos(\phi) \quad (3.6)$$

$$h_+ = \frac{4(GM)}{rC^2} \left(\frac{\pi f(t)}{c} \right)^{2/3} \cos \sin(\phi) \quad (3.7)$$

where $M = \mu^3 M^{2/5}$. If we also define the characteristic Radius $\frac{2GMc}{c^2}$ and wavelength $\lambda = c/f_{gw}$, where f_{gw} is the frequency of the GW, evaluating at the retarded time, with an arbitrary phase factor, we get

$$h_+(t) = A \frac{1 + \cos}{2} \cos(2\pi f_{gw} t_{ret} + 2\phi) \quad (3.8)$$

$$h_x(t) = A \cos \sin(2\pi f_{gw} t_{ret} + 2\phi) \quad (3.9)$$

where φ is phase, f_g is the frequency and T is the time period in the rotation.

3.3.1 Energy loss for circular orbits

Calculating the derivatives of Eq. [5.3.28] can be rather tedious since both d and a are time dependent. The calculation, as well as the result, simplify drastically if one instead considers circular orbits, $a = a$ and the angular velocity is constant. If we calculate the third time derivative of Eq. [5.3.28] with these conditions we obtain Equation [5.3.29]. In this representation, h is given as Eq. [5.3.27] and m is kept constant. We can now insert this result in Eq. [5.3.22] together with Eq. [5.3.24] for the reduced mass of the system in order to calculate the gravitational radiation luminosity L . This falls out as

$$L = h \frac{dE}{dt} i = \frac{32m^3M^2(M+m)}{5Gd^3} \quad (3.10)$$

where hi denotes the average taken over one period. We get

$$L = h \frac{dE}{dt} i = \frac{32m^3c^5M^2(M+m)}{5Gd^3} \quad (3.11)$$

3.3.2 Correction for elliptical orbits

As stated in the previous section, taking the time derivatives of the components of the quadrupole tensor for a general elliptical orbit can be quite tedious. This was however done once and for all in 1963 by P. C. Peters and J. Matthews [13]. Taking the time derivatives of Eq. [5.3.28], averaging over one period and plugging it into Eq. [5.3.22] we then, for a general SM

binary system, obtain the luminosity as

$$L_{\text{elliptical}} = L_{\text{circular}} f(\varepsilon) = \frac{32m^2c^5M^2(M+m)}{5a(1-\varepsilon)^{7/2}} \quad 1 + \frac{73}{24}\varepsilon^2 + \frac{37}{96}\varepsilon^4 \quad (3.12)$$

where a where the semi-major axis and

$$f(\varepsilon) = \frac{1}{(1-\varepsilon)^{7/2}} \quad 1 + \frac{73}{24}\varepsilon^2 + \frac{37}{96}\varepsilon^4 \quad (3.13)$$

is a correction factor depending only on the eccentricity of orbital motion. We see in figure 3.2 that this factor can be quite significant when the eccentricity is large. For most planetary systems in the solar system however the orbits are almost circular and $\varepsilon \approx 1$. Again, if we want to express the luminosity in SI-units, we can use the conversion factor Eq. [5.3.23][5].

3.4 Eccentric Binary Inspiral Evolution

The evolution of compact binary coalescences can be broken into three phases: inspiral, merger, and ringdown. We focus on the inspiral phase, as once the CBC enters merger eccentricity no longer produces distinguishable effects. The inspiral phase is the longest phase in a CBC, ending when the objects reach their innermost stable circular orbit (ISCO). This occurs at the following condition for semi-major axis length $a[1]$:

$$a_{\text{ISCO}} = 6 \frac{G(m_1 + m_2)}{c^2} \quad (3.14)$$

In his paper Gravitational Radiation from Post-Newtonian Sources and Inspiring Compact Binaries, Luc Blanchet derives the following coupled lowest order ordinary differential equations describing period decay and

eccentricity decay of a BBH during the inspiral phase[4]:

$$P_{orb} = -\frac{192\pi}{5\epsilon} \left(\frac{2\pi G}{P_{orb}}\right)^{5/2} \frac{m_1 m_2}{(m_1 + m_2)^{1/3}} \frac{1}{(1 - \epsilon)^{7/2}} \quad 1 + \frac{73}{24}\epsilon^2 + \frac{37}{96}\epsilon^4 \quad (1-\epsilon)^{-7/2} \quad (3.15)$$

$$\epsilon = -\frac{608\pi e}{15\epsilon P_{orb}} \frac{m_1 m_2}{(m_1 + m_2)^{1/3}} (1 + \frac{121}{304}\epsilon^2)(1 - \epsilon)^{-5/2} \quad (3.16)$$

It is important to note that these equations ignore spin effects and higher order effects such as spin precession or higher order modifications. DeSachet integrates analytically to determine that orbital period and eccentricity are related via[1,11]

$$C_0 P^{19/9} = \frac{\epsilon^2}{(1 - \epsilon)^{19/6}} (1 + \frac{121}{304}\epsilon^2)^{145/121} \quad (3.17)$$

where C_0 is a constant determined by the initial conditions of the orbit.

Numerically solving (3.22) and (3.23) with the initial conditions of $\epsilon_0 = 0.4$ and $P_{orb,0} = 0.1$ yields the time series for orbital period and eccentricity shown in Figure 3.2. Additionally, a time series for semi-major axis length a was calculated from Kepler's Third Law (also seen in Figure 3.2)[1],

$$a = [P_{orb}^2 \left(\frac{G(m_1 + m_2)}{4\pi^2}\right)]^{1/3} \quad (3.18)$$

The shape of the time series' for orbital period and eccentricity depend on initial orbital period, initial eccentricity, chirp mass, and mass ratio. As initial eccentricity, or for our purposes, the eccentricity at an orbital period of 0.1s (corresponding to the lowest frequency in the LIGO band) increases, the duration of the CBC in the LIGO band decreases. As the BBH reaches ISCO in a shorter amount of time. As total mass increases and/or mass ratio decreases, the duration of the BBH in the LIGO band also decreases.

These patterns can be seen in Figures 3.4, 3.5, and 3.6.

3.5 Waveform Models

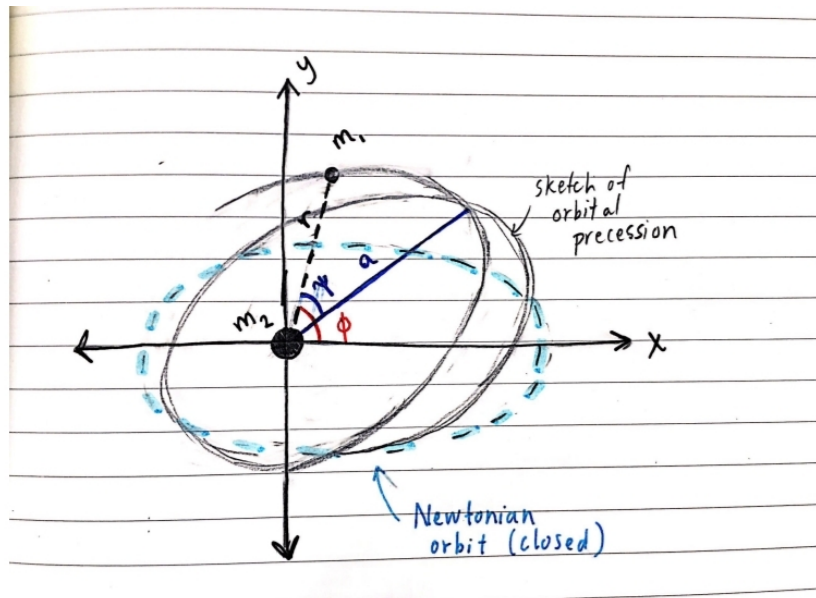
Once a dynamically captured BH pair is in eccentric orbit, a burst is theorized to be emitted every time the pair passes at a close encounter (i.e. at periastron). This causes the semi-major axis (a) and eccentricity (e) to decrease with time, while orbital frequency increases with time. If sufficient energy is lost through gravitational radiation, the BH pair will merge.

Gravitational wave strain, $h(t)$ is generated by an accelerating quadrupole moment, $\mathbf{M}(t) \sim \frac{d^2}{dt^2}(\mathbf{I})$ where $\mathbf{I} = \rho r^2 dV$. Without taking the effects of eccentricity into account, the strain is optimized in (3.26) where d is the distance to the source, a is the distance between the orbiting bodies, m_1 and m_2 are the masses of the BH, and $\phi(t)$ is the phase evolution:

$$h(t) = \frac{2G(m_1 + m_2)}{c^2 d} \quad \frac{2G(m_1 + m_2)}{c^2 a} \cos(2\phi(t)) \quad (3.19)$$

However, BBH in eccentric orbits produce a more complicated GW strain, due to emitting GW bursts at periastron, periastron precession, and the consequent oscillating distance between the orbiting bodies. The location of a body in an eccentric orbit can be defined using two angles: ψ and ϕ . ψ , also known as the true anomaly, corresponds to the radial period; it is taken with respect to the semi-major axis. However, due to periastron precession, the semi-major axis is itself rotating. It takes this into account; it corresponds to the orbital period taken from a fixed axis in space, while the axis from which it is taken is rotating. See Figure 3.7 for a visualization[1].

Taking these effects into account, the plus and cross polarizations for

**Figure 3.2**

gravitational wave strain from an eccentric BBH system are[1]:

$$\begin{aligned}
 h_+(t) = & \frac{\mu}{2D} ([1 - 2\cos(2\theta)c \\
 & \cos^2(\varphi(t)) - 3\cos(2\varphi(t))]r(t) + \\
 & (3 + \cos(2\theta)) [2\cos(2\varphi(t))\varphi(t)\dot{\varphi}(t)]r^2(t) \\
 & + [4(3 + \cos(2\theta)) \sin(2\varphi(t))\dot{\varphi}(t)r(t) + \\
 & (1 - 2\cos(2\varphi(t))\dot{\varphi}(t) - 3\cos(2\varphi(t))\ddot{\varphi}(t)]r(t) \quad (3.20)
 \end{aligned}$$

$$h_x(t) = \frac{2\mu\cos(\theta)}{D} \quad (3.21)$$

where μ is the reduced mass of the binary, D is the distance to the source, θ is the angle of inclination of the source, r is the distance between the two BHs, and φ is angle corresponding to the orbital period [9,1].

To solve for the strain, we need to time evolve ψ , which is done using the energy and angular momentum of the system. In the derivation we use the Newtonian approximations of these quantities. The Newtonian definition of orbital energy for an elliptical orbit with total mass M_{tot} , reduced mass μ , and semi-major axis length a is, in Joules[1]:

$$E_{orb} = K + U = \frac{U}{2} - \frac{GM_{tot}\mu}{2a} \quad (3.22)$$

where $K + U = \frac{U}{2}$ is the Virial Theorem for gravity. The Newtonian definition of orbital angular momentum is as follows, in $Kg^2 m/s$ [1]:

$$L_{orb} = GM_{tot}(1 - e)^{-1/2} \quad (3.23)$$

From these definitions we can express the quantities of specific total energy and specific angular momentum in geometric units ($= c = 1$), to be used throughout :

$$E = 1 + \frac{E_{orb}}{\mu}, L = \frac{L_{orb}}{\mu} \quad (3.24)$$

The distance r between the two BH's is:

$$r = \frac{a(1-e^2)}{1 + e\cos(\psi)} \quad (3.25)$$

where ψ is the true anomaly of the eccentric system (see Figure 3.8). To generate a time series for r , we must time evolve using the following equation, adapted from [1,9]:

$$\psi = \frac{(1 - E^2)^{1/2}}{V_t(1 - e)} [a(1 - e) - C_0(1 - e) - ea(1 - e)^2] - eC_0(1 - e)\cos(\psi) \quad (3.26)$$

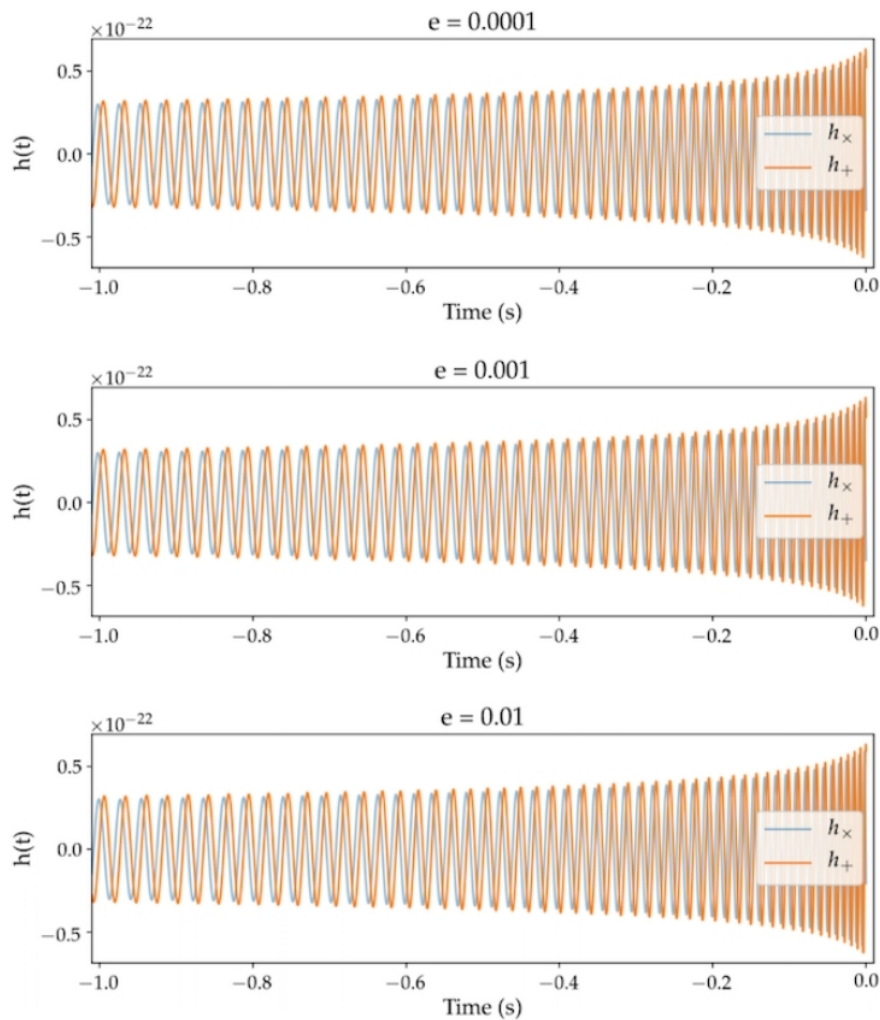


Figure 3.3

where the constant C_0 is given by :

$$C_0 = \frac{2}{1 - E^2} - 2a \quad (3.27)$$

and the potential V_t is given by:

$$V_t = \frac{Er^4}{r^2 - 2r} \quad (3.28)$$

Finally, to solve the gravitational wave strain equations given in (3.27) and (3.28), we must generate a time series for angle describing where a body is in its orbit over period (see Figure 3.8). This is achieved with the following relationship between specific angular momentum, and potential V_t [1,9]:

$$\varphi = \frac{L}{V_t} \quad (3.29)$$

Choosing an initial period and eccentricity, solving for the time evolution of r and φ , and substituting into (3.27) and (3.28) yields the time series shown in Figure 3.9. This model shows the unique feature appearing in a waveform generated by a BBH system in an eccentric orbit: bursts of gravitational wave radiation produced at periastron passage. As orbital eccentricity increases, these bursts increase in magnitude. Additionally, just like non-eccentric waveforms, this model shows the characteristic chirp behavior of a CBC: amplitude and frequency of the GW strain increase as the binary evolves.

3.6 Results

Numerically solving equations (3.22) and (3.23) with different initial conditions of P_{orb} and e yields the time series for orbital period and eccentricity. Which can be done by the python using the libraries "scipy.integrate" as an the differential equation solver which directly call the function to the

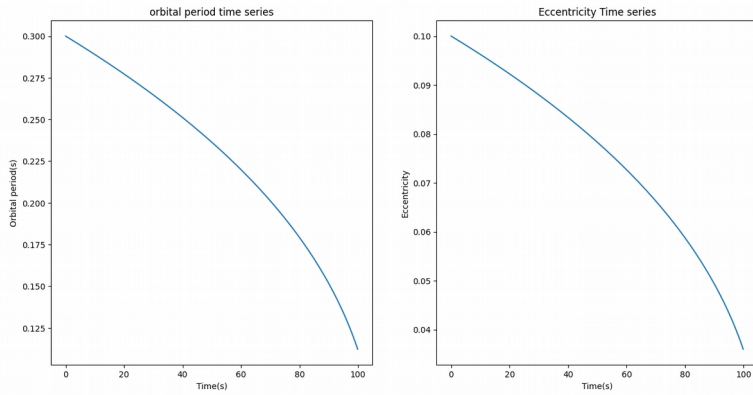


Figure 3.4 The figure for initial eccentricity = 0.1s and the orbital period = 0.3s

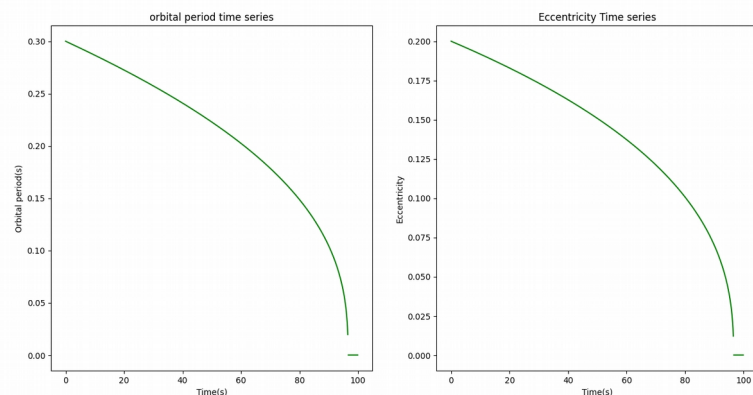


Figure 3.5 The figure for initial eccentricity = 0.2s and the orbital period = 0.3s

module then solve using initial conditions, To plot the corresponding values "matplotlib.pyplot" and to handle this huge amount of data we use "numpy" modulesLet's the corresponding graphs for different initial conditions as,

For the eccentricity change to = 0.2s and the orbital period is constant as 0.3s which show that when the eccentricity increases the orbital period and eccentricity decreasing to a time of nearly 90s after the remains constant for the all other time series shown in the figure (B10) we eccentricity

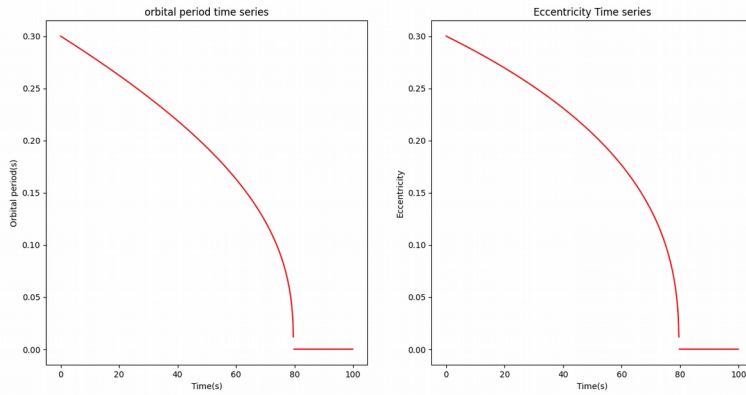


Figure 3.6: The figure for initial eccentricit = 0.2s and the orbital period = 0.3s

Figure 3.7: orbital period constant and eccentricity varry

increases to the =0.3s we see that the orbital period and eccentricity decreasing to a time of nearly 80s after the remains constant for the all other time series shown in the figure(3.11).

Lets make the orbital period as constant = 0.1s and the varry the initial eccentricity from 0.1s to 1s by the increment of the 0.1s we get the figure as shown in the figure (3.12).

Orbital period time series and eccentricity time series with varying total masses and All series have a mass ratio of 1 we get the figure as shown in the figure (3.5)Orbital period time series and eccentricity constant with varying massses ratio 1

Once a dynamically captured BH pair is in eccentric orbit, a GW burst is theorized to be emitted every time the pair passes at a close encounter (i.e. at periastron)This causes the semi-major axis (a) and eccentricity (e) to decrease with time, while orbital frequency increases wAffetisue. cient energy is lost through gravitational radiation, the BH pair will merge.

The shape of the time series for orbital period and eccentricity depend on initial orbital period, initial eccentricity, chirp mass, and mass ratio.

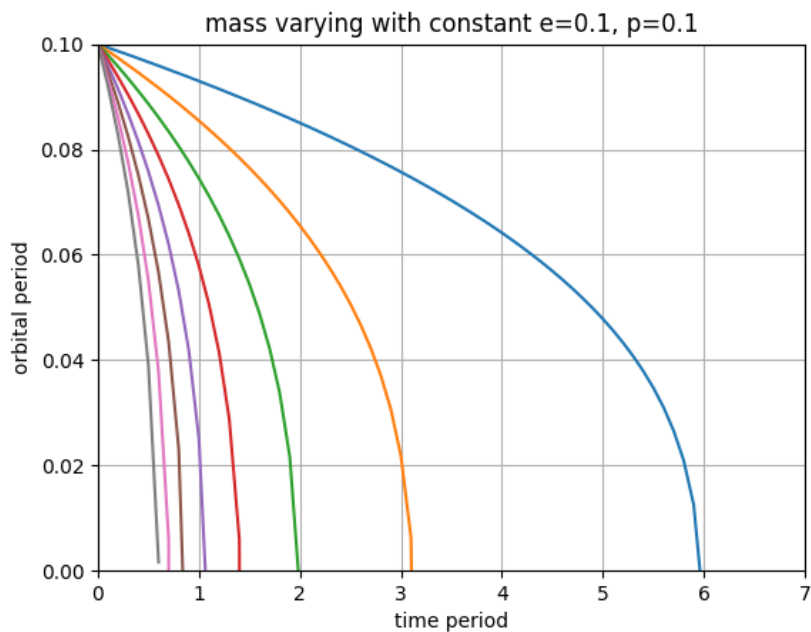


Figure 3.8 Orbital and eccentricity constant mass ratio vary as 1

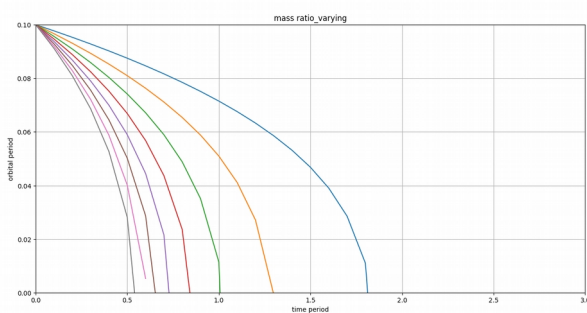


Figure 3.9 mass ratio vary

initial eccentricity, or for our purposes, the eccentricity at an orbital period of 0.1s (corresponding to the lowest frequency in the LIGO band) increases, the duration of the CBC in the LIGO band decreases. As BBH reaches ISCO in a shorter amount of time. As total mass increases and/or mass ratio decreases, the duration of the BBH in the LIGO band also decreases.

3.6.1 Generating a Waveform Model using Python

Gravitational wave strain, $h(t)$ is generated by an accelerating quadrupole moment, I : Without taking the effects of eccentricity into account, this strain is optimized in (6) where d is the distance to the source, a is the distance between the orbiting bodies, and m_1, m_2 are the masses of the bodies. $\phi(t)$ is the phase evolution using the equation 3.27,3.28 with initial orbital period $P_0 = 01s$ and initial eccentricities $e=0.1$.

But what we exactly need as shown in the figure (3.17,3.18).

3.7 Working code

We use the python as well as the mathematica software for plotting the corresponding graphs. The modules are "numpy", "matplotlib.pyplot" and "scipy.integrate import odeint".

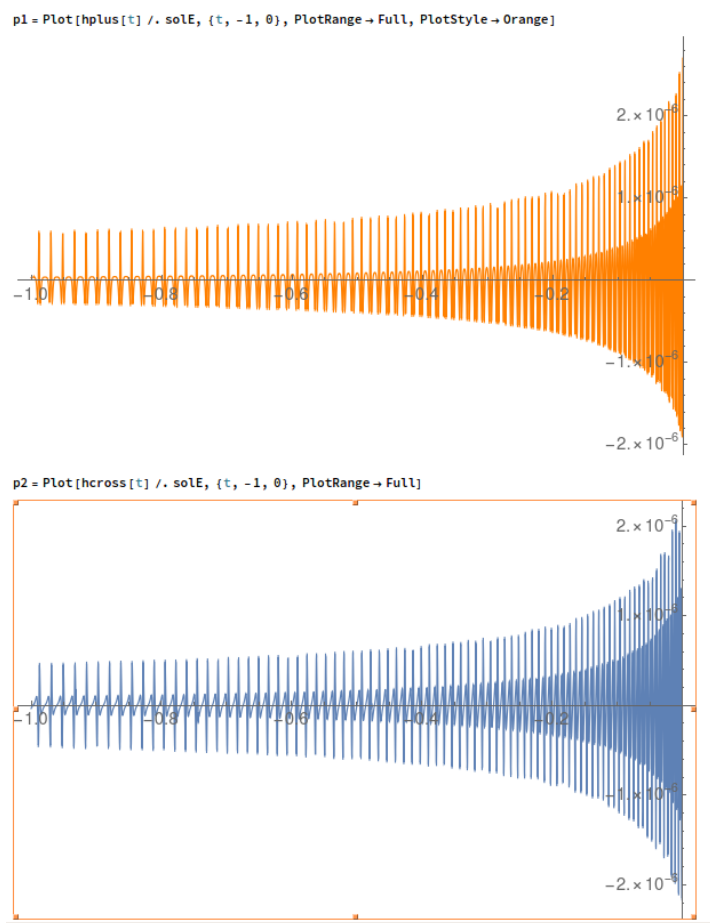


Figure 3.10 h_{plus} and the cross polarization for the initial eccentricity 0.1

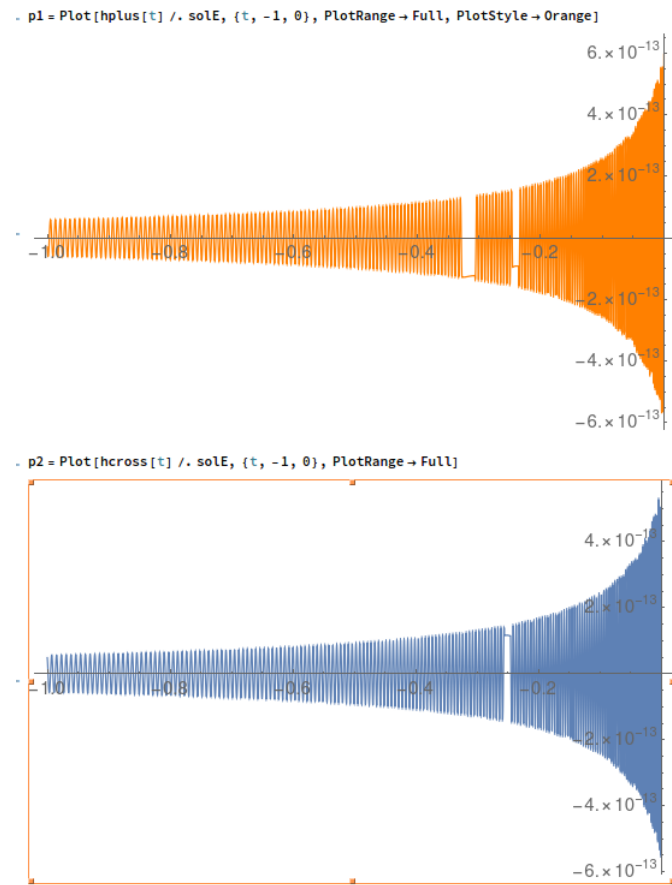


Figure 3.11 Plus and the cross polarization for the initial eccentricity 0.1

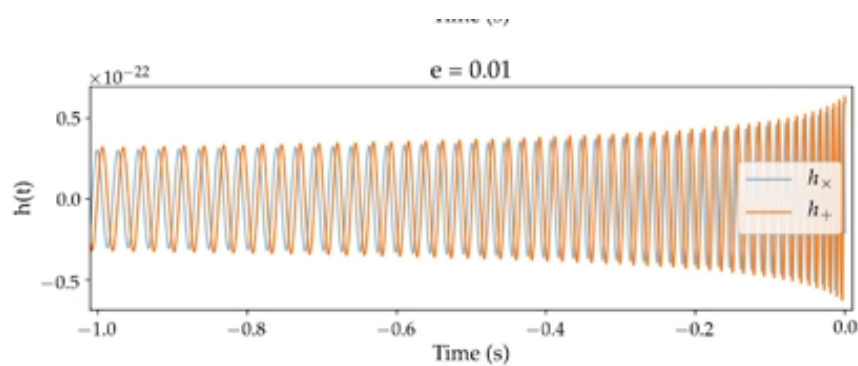


Figure 3.12 With initial orbital period $P_0 = 01s$ and initial eccentricities $e_0=0.1$ 'This figure is taken from [Modeling and Measuring Eccentricity in Binary Black Hole Inspirals]'

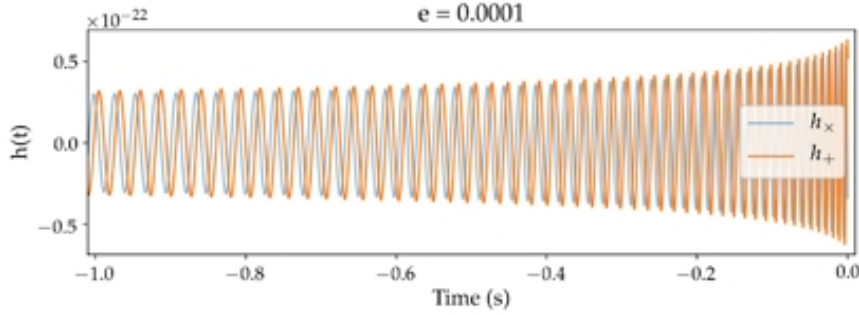


Figure 3.13 With initial orbital period $P_0 = 01\text{s}$ and initial eccentricities $e_0=0.0001$ 'This figure is taken from [Modeling and Measuring Eccentricity in Binary Black Hole Inspirals]'

```

from matplotlib.pyplot import*
from numpy import*
from scipy.integrate import odeint
def f(x,t):
    p,e= x
    p1=(-192*3.14/(5*(c**5)))
    p2=(2*3.14*G/(p))**(5/3)
    p3=m1*m2/((m1+m2)**(1/3))
    p4=(1+((73/24)*e**2)+((37/96)*e**4))/((1-e**2)**(7/2))
    e1=(-608*3.14/(15*(c**5)))
    e2=e/p
    e3=(2*3.14*G/(p))**(5/3)
    e4=m1*m2/((m1+m2)**(1/3))
    e5=(1+((121/304)*e**2))/((1-e**2)**(5/2))
    a=p1*p2*p3*p4
    b=e1*e2*e3*e4*e5
    q=a/b

    return[a,b]
m1=10*1.989*10**30      # initial conditions
m2=10*1.989*10**30
c=3*10**8
G=6.6743*10**-11
#q=linspace[0.0,0.4,.1]
#w=linspace[0.0,0.3,.1]
x=[0.3,0.3]
t=arange(0,100,.10)
sol=odeint (f,x,t)
#figure(1)
fig,ax=subplots(nrows=1,ncols=2)
ax[0].set_ylabel("Orbital period(s)")
ax[0].set_xlabel("Time(s)")
ax[0].set_title("orbital period time series")
ax[0].plot(t,sol[:,0],color="r")
#ylim(0,.30)
#figure(2)
ax[1].set_xlabel("Time(s)")
ax[1].set_ylabel("Eccentricity")
ax[1].set_title("Eccentricity Time series")
#ylim(0,.12)
ax[1].plot(t,sol[:,1],color="r")
show()

```

Figure 3.14 Program for the eccentricity and the orbital period

```

From numpy import*
From matplotlib import*
def f(p,e):
    pi=3.141592653589793
    c=p**2/(1-e**2)
    m1=1.329*1.14*(3**e**3)**3*(2**3.14*p)**(5/3)*(m1*m2/(m1+m2))**(1/3)*(1+(73/24)*e**2+(37/96)*e**4)*(1-e**2)**(-7/2)
    m2=1.329*1.14*(155*(c**5))**3
    e2=e*p
    e3=e*p**2
    e4=e*p**3
    e5=e*p**4
    e6=e*p**5
    e7=e*p**6
    e8=e*p**7
    e9=e*p**8
    e10=e*p**9
    e11=e*p**10
    m1=2.01_98910**30
    m2=1.9910**30
    e3=1.0
    d=6.4741**10**11
    h=1.0
    h1=1.0
    p0=1.0
    e_var=range(0,1,0.01)
    t_var=range(0.0,100,0.1)
    for e in e_var:
        t=0.0
        t+=h
        while t<=t_var[-1]:
            if t>t_var[-1]:
                t=t-var
            tlist.append(t)
            elist.append(e)
            plist.append(m1)
            eewh=f(p,e)
            p+=eewh*t
            t+=h
    point=tlist
    xlist=(e_var)
    ylist=(tlist)
    elist=reshape(elist)
    plist=reshape(plist)
    tlist=reshape(tlist)
    xlist=reshape(xlist,int(y/x))
    elist=reshape(elist,int(y/x))
    plist=reshape(plist,int(y/x))

```

Figure 3.15 Orbital period constant with varying eccentricity'1'

```

figure(1)
for i in range(x):
    plot (tlist[i],plist[i])
grid("true")
xlabel("time period")
xlim(0,7)
ylim(0.00,.10)
ylabel("orbital period")
title("Ecc varying graph")
legend()
#show()
#figure(2)
plot(tlist,elist)
xlim(0,7)
ylim(0.00,.10)
show()
|

```

Figure 3.16 Orbital period constant with varying eccentricity'2'

```

from numpy import*
from matplotlib.pyplot import*
def f(p,e,m):
    m1=m
    m2=m
    p1=(-192*3.14/(5*c**5))*(2*3.14*G/p)**(5/3)*(m1*m2/(m1+m2)**(1/3))*(1+(73/24)*e**2+(37/96)*e**4)*(1-e**2)**(-7/2)
    return p1

def g(p,e,m):
    m1=m
    m2=m
    e1=(-608*3.14/(15*(c**5)))
    e2=e/p
    e3=(2*3.14*G/(p))**(5/3)
    e4=m1*m2/((m1+m2)**(1/3))
    e5=(1+((121/304)*e**2))/((1-e**2)**(5/2))
    e7=e1*e2*e3*e4*e5
    #e1=(-608*3.14*e/(15*c**5*p))*(m1*m2/(m1+m2)**(1/3))*(1+(121/304)*e**2)*(1-e**2)**(-5/2)
    return e7

plist=[]
elist=[]
tlist=[]
ms=1.989*10**30
c=3*10**8
G=6.6743*10**-11
#e=0.1
h=.10
t=0.0
p=0.1
e=0.1

m_var=arange(10,50,5)
m_var=m_var**ms
t_var=arange(0.0,100,0.1)
for m in m_var:
    e=0.1
    p=0.1
    t=0.00
    for t in t_var:
        tlist.append(t)
        elist.append(e)
        plist.append(p)
        e=e+h*f(p,e,m)
        p=p+h*f(p,e,m)
        t=t+h

```

Figure 3.17 Orbital period and the eccentricity constant with varying the masses'1'

```

m_var=arange(10,50,5)
m_var=m_var*ms
t_var=arange(0.0,100,0.1)
for m in m_var:
    e=0.1
    p=0.1
    t=0.00
    for t in t_var:
        tlist.append(t)
        elist.append(e)
        plist.append(p)
        e=e+h*f(p,e,m)
        p=p+h*f(p,e,m)
        t=t+h

y=len(tlist)
x=len(m_var)
tlist=array(tlist)
elist=array(elist)
plist=array(plist)

tlist=tlist.reshape(x,int(y/x))
elist=elist.reshape(x,int(y/x))
plist=plist.reshape(x,int(y/x))

figure(1)
for i in range(x):
    plot (tlist[i],plist[i])

grid("true")
xlabel("time period")
xlim(0,7)
ylim(0.00,.10)
title("mass varying with constant e=0.1, p=0.1")
ylabel("orbital period")

#show()
#figure(2)
#plot(tlist,elist)
##xlim(0,7)
##ylim(0.00,.10)
#show()

```

Figure 3.18Orbital period and the eccentricity constant with varying the masses'2'

```

from numpy import*
from matplotlib.pyplot import*
def f(p,e,m1,m2):
    p1=(-192*3.14/(5*c**5))*(2*3.14*G/p)**(5/3)*(m1*m2/(m1+m2)**(1/3))*(1+(73/24)*e**2+(37/96)*e**4)*(1-e**2)**(-7/2)
    return p1
def g(p,e,m1,m2):
    e1=(-608*3.14/(15*(c**5)))
    e2=e
    e3=(3/3.14*c/(p))**(5/3)
    e4=m1*m2/((m1+m2)**(1/3))
    e5=(1+((121/304)*e**2))/((1-e**2)**(5/2))
    e7=e1*e2*e3*e4*e5
    #e1=(-608*3.14*(p/(15*c**5)))*(m1*m2/(m1+m2)**(1/3))*(1+(121/304)*e**2)*(1-e**2)**(-5/2)
    return e7
plist=[]
elist=[]
tlist=[]
ms=1.989*10**30
c=3*10**8
G=6.6743*10**-11
#e=0.1
h=.10
t0_0
p0_0
e0_0
m1=50*ms
m_var=arange(10,50,5)
m_var=m_var*ms
t_var=arange(0.0,100,0.1)
for m2 in m_var:
    e=0.1
    p=0.1
    t=0.00
    for t in t_var:
        tlist.append(t)
        elist.append(e)
        plist.append(p)
        ee=h*f(p,e,m1,m2)
        pep=h*f(p,e,m1,m2)
        t=t+h
    t=t+h

```

Figure 3.19 Orbital period and the eccentricity constant with varying the masses ratio '1'

```

y=len(tlist)
x=len(m_var)
tlist=array(tlist)
elist=array(elist)
plist=array(plist)

tlist=tlist.reshape(x,int(y/x))
elist=elist.reshape(x,int(y/x))
plist=plist.reshape(x,int(y/x))

figure(1)
for i in range(x):
    plot (tlist[i],plist[i])

grid("true")
xlabel("time period")
xlim(0,3)
ylim(0.00,0.10)
ylabel("orbital period")
title("mass ratio_varying")
#show()
#figure(2)
#plot(tlist,elist)
##xlim(0,7)
##ylim(0.00,.10)
show()
|

```

Figure 3.20 Orbital period and the eccentricity constant with varying the masses'2'

3.7. WORKING CODE

47

```

Ntot = 40 + 1.98*1010; m1 = 20 + 1.98*1010; m2 = 20 + 1.98*1010; g = 6.67*10-11; c = 3*108; μ =  $\frac{m_1 \cdot m_2}{m_1 + m_2}$ ;
r0 = 3.086*103; e0 = 0.25; P0 = 0.1;
a0 =  $\left( \frac{P_0^2}{4} + \frac{c^2}{μ^2} \cdot (m_1 + m_2) \right)^{1/2}$ 
1.10195*103
ω0 =  $\frac{G \cdot Ntot}{a0^3}$ 
394784.
FindRoot[u == e0*Sin[u], {u, 0}]
(u == 0.)
N[ $\frac{\cos(\theta) - e0}{1 - e0 \cdot \cos(\theta)}$ ]
1.

Solve[θ == u - e0*Sin[u], u]
-- Solve[θ == u - e0*Sin[u], u]
Solve[θ == u - 0.1*Sin[u], u]
{u == 0.1}
e0 =  $\frac{(1 - e(t)^2) \cdot a'(t)}{c^2} \cdot (e^2(t) - \sqrt{\frac{g \cdot (m_1 + m_2)}{a(t)^3}} \cdot (1 - e(t)^2)^{-3/2} \cdot (1 + e(t) \cdot \cos(e(t)))^2)$ 
 $\frac{a(t) \cdot (1 - e(t)^2)}{c^2} = 1$ 
θ0 = Cos[ $\frac{(1 - e(t)^2) \cdot a'(t)}{c^2} - e0$ ]
-1.52752
solE = NDsolve[{r'(t) ==  $\frac{(1 - e(t)^2) \cdot a'(t)}{1 + \cos(e(t)) \cdot e(t)}$ ,  $\frac{2 \cdot a(t) \cdot e(t) \cdot e'(t)}{1 + \cos(e(t)) \cdot e(t)}$ ,  $\frac{a(t) \cdot (1 - e(t)^2) \cdot (\cos(e(t)) \cdot e'(t) - e(t) \cdot \sin(e(t)) \cdot e''(t))}{1 + \cos(e(t)) \cdot e(t)^2}$ , θ'(t) ==  $\sqrt{\frac{g \cdot (m_1 + m_2)}{a(t)^3}} \cdot (1 - e(t)^2)^{-3/2} \cdot (1 + e(t) \cdot \cos(e(t)))^2$ , a''(t) ==  $\frac{-64}{5} \frac{c^2}{\mu^2} \frac{m_1 \cdot m_2 \cdot (m_1 + m_2)}{a(t)^5} \cdot \left(1 + \frac{73}{24} \frac{e(t)^2}{c^2} + \frac{37}{96} e(t)^4\right) \cdot (1 - e(t)^2)^{-5/2}$ , r[0] == r0, θ[0] == θ0, a[0] == a0}, {r, θ, e, a}, {t, -10, 1}]
{{r -> InterpolatingFunction[ $\boxed{\text{Domain: } [-10, 1]} \rightarrow \text{Output: scalar}$ ], θ -> InterpolatingFunction[ $\boxed{\text{Domain: } [-10, 1]} \rightarrow \text{Output: scalar}$ ], e -> InterpolatingFunction[ $\boxed{\text{Domain: } [-10, 1]} \rightarrow \text{Output: scalar}$ ], a -> InterpolatingFunction[ $\boxed{\text{Domain: } [-10, 1]} \rightarrow \text{Output: scalar}$ ]}}
{{r -> InterpolatingFunction[ $\boxed{\text{Domain: } [-20, 0]} \rightarrow \text{Output: scalar}$ ], θ -> InterpolatingFunction[ $\boxed{\text{Domain: } [-20, 0]} \rightarrow \text{Output: scalar}$ ], e -> InterpolatingFunction[ $\boxed{\text{Domain: } [-20, 0]} \rightarrow \text{Output: scalar}$ ], a -> InterpolatingFunction[ $\boxed{\text{Domain: } [-20, 0]} \rightarrow \text{Output: scalar}$ ]}}
{{r -> InterpolatingFunction[ $\boxed{\text{Domain: } [0, 10]} \rightarrow \text{Output: scalar}$ ], θ -> InterpolatingFunction[ $\boxed{\text{Domain: } [0, 10]} \rightarrow \text{Output: scalar}$ ], e -> InterpolatingFunction[ $\boxed{\text{Domain: } [0, 10]} \rightarrow \text{Output: scalar}$ ], a -> InterpolatingFunction[ $\boxed{\text{Domain: } [0, 10]} \rightarrow \text{Output: scalar}$ ]}}

```

Figure 3.21For the polarisation'1'

```

σ =  $\frac{π}{4}$ ; Dis = 3.08257*1017 (*instance of GM158914*)
3.08257*1017
hplus[t] =  $\frac{G \cdot μ}{c^4 \cdot 2 \cdot Dis} \cdot ((1 - 2 \cdot \cos(2 \cdot σ) \cdot \cos(e(t)))^2 - 3 \cdot \cos(2 \cdot φ(t)) \cdot r'(t)^2 + (3 + \cos(2 \cdot σ)) \cdot (2 \cdot \cos(2 \cdot φ(t)) \cdot φ'(t))^2 + \sin(2 \cdot φ(t)) \cdot φ''(t)) \cdot r(t)^2 + (4 \cdot (3 + \cos(2 \cdot σ)) \cdot \sin(2 \cdot φ(t)) \cdot φ'(t) \cdot r'(t) + (1 - 2 \cdot \cos(2 \cdot σ) \cdot \cos(e(t)))^2 - 3 \cdot \cos(2 \cdot φ(t)) \cdot r''(t)) \cdot r(t)$ 
2.64462*10-31 ((1 - 3 \cdot \cos(2 \cdot φ(t))) \cdot r'(t)^2 + r(t) \cdot (12 \cdot \sin(2 \cdot φ(t)) \cdot r'(t) \cdot φ'(t) + (1 - 3 \cdot \cos(2 \cdot φ(t))) \cdot r''(t)) + 3 \cdot r(t)^2 \cdot (2 \cdot \cos(2 \cdot φ(t)) \cdot φ'(t)^2 + \sin(2 \cdot φ(t)) \cdot φ''(t)))
hcross[t] =  $\frac{2 \cdot μ \cdot \cos(σ) \cdot G}{Dis \cdot c^4} \cdot ((\sin(2 \cdot φ(t)) \cdot r'(t))^2 + (\cos(2 \cdot φ(t)) \cdot φ'(t))^2) \cdot r(t)^2 + (4 \cdot \cos(2 \cdot φ(t)) \cdot φ'(t) \cdot r'(t) + \sin(2 \cdot φ(t)) \cdot r''(t)) \cdot r(t)
-7.48011*10-31 (\sin(2 \cdot φ(t)) \cdot r'(t)^2 + r(t) \cdot (4 \cdot \cos(2 \cdot φ(t)) \cdot r'(t) \cdot φ'(t) + \sin(2 \cdot φ(t)) \cdot r''(t)) + r(t)^2 \cdot (-2 \cdot \sin(2 \cdot φ(t)) \cdot φ'(t)^2 + \cos(2 \cdot φ(t)) \cdot φ''(t)))
p1 = Plot[hplus[t] /. solE, {t, -10, 1}, PlotStyle -> Orange, PlotRange -> Full]$ 
```

Figure 3.22For the polarisation'2'

Chapter 4

PyCBC

We will be using the PyCBC library, which is used to study gravitational-wave data, find astrophysical sources due to compact binary mergers, and study their parameters. These are some of the same tools that the LIGO and Virgo collaborations use to find gravitational waves in LIGO/Virgo data. In this chapter we will walk through how to get information about the catalog of binary mergers programmatically, and also how to read in detector strain data around each event from the full open data set released for LIGO's first observing run.

4.1 The software environment setup

PyCBC is installable through pip, but also relies on portions of the LALSuite c-library. A bundled version of this suitable for use with PyCBC is also available on Mac / Linux through pip. These can be installed as follows within the notebook.

```
import sys
!{sys.executable} -m pip install pycbc ligo-common --no-cache-dir
```

Figure 4.1 pip-comment-for-pycbc

```

# Either from the catalog as a whole
c = catalog.Catalog()
mchirp = c.medianid('mchirp')
print(mchirp)

# or from a specific merger
m = catalog.Merger("GW170817")
mchirp_gw170817 = m.medianid('mchirp')
print("GW170817: {}".format(mchirp_gw170817))

# print parameters that can be read
print(m.data.keys())

```

[15.2 7.9 35.7 28.6 8.9 24.2 1.186 21.5 25. 26.7
29.3]
GW170817: 1.186
[u'files', u'distance', u'a_final', u'mass1', u'tc', u'far_gstlal', u'far_pycbc', u'mass2', u'mchirp', u'snr_gstlal', u'redshift', u'far_cwb', u'utctime', u'L_peak', u'sky_size', u'mfinal', u'E_rad', u'chi_eff', u'snr_pycbc', u'snr_cwb']

Figure 4.2 Getting parameters

4.1.1 How can I get parameters?

One can also retrieve some of the basic parameters of each source from the catalog directly as follows. Note that all parameters are given in the source frame. This means that they include the effect of redshift. The parameters either from the catalog as a whole or from a specific merger shown in figure(4.3).

4.2 Catalog of Binary Mergers

PyCBC provides an API to look at the catalog of binary mergers. This consists of 55 binary black hole mergers and the two binary neutron star mergers GW170817 and GW190425. The key information such as the 'chirp' mass of a binary merge can be retrieved.

4.2.1 What binary mergers are in the catalog?

This module consists of large number of the gravitational waves merger signals. Lets see how to import the module and the list of mergers in the catalog, figure(4.1).

4.3. ACCESSING LIGO/VIRGO DATA AROUND SPECIFIC BINARY MERGER IN THE CATALOG

```
from pycbc import catalog

### List the mergers in the catalog
for merger_name in catalog.Catalog():
    print(merger_name)
```

```
GW151012
GW170608
GW170729
GW150914
GW151226
GW170814
GW170817
GW170104
GW170809
GW170818
GW170823
```

Figure 4.3Mergers information

4.2.2 Transform Mass Parameters into the Detector Frame

By default the above interface returns parameters in the source frame. Due to cosmological redshift gravitational-waves are stretched as they travel. This causes the observed waveform to be different in the detector frame. This corresponds to an observed change in the mass parameters (for example). However, the relationship is fairly straightforward shown in figure(4.4).

4.3 Accessing LIGO/Virgo data around Specific Binary Merger in the Catalog

In this section, we will look into how to read detector data from the LIGO and Virgo instruments using the PyCBC APIs. It is possible to both get

4.3. ACCESSING LIGO/VIRGO DATA AROUND SPECIFIC BINARY MERGER IN THE CATALOG

```
m = catalog.Merger('GW150914')
source_mchirp = m.medianid('mchirp')
redshift = m.medianid('redshift')
det_mchirp = source_mchirp * (1 + redshift)

print('Chirp Mass of GW150914')
print('Source Frame: {} Solar Masses'.format(source_mchirp))
print('Detector Frame: {} Solar Masses'.format(det_mchirp))
```

Chirp Mass of GW150914
Source Frame: 28.6 Solar Masses
Detector Frame: 31.174 Solar Masses

Figure 4.4 Transform Mass Parameters into the Detector Frame

```
%matplotlib inline

import pylab

m = catalog.Merger("GW150914")

# Get the time series data around GW150914 from Hanford
# 'ts_han' is a pycbc.types.TimeSeries object which contains
# gravitational-wave strain in this instance and has metadata
# such as the start time, and sample rate.
ts_han = m.strain('H1')

# And now Livingston
ts_liv = m.strain('L1')

# We can see how much data was returned and its boundaries
# Note: All times are given in seconds since the GPS time epoch
print("Duration: {} Start: {} End: {}".format(ts_han.duration,
                                              int(ts_han.start_time),
                                              int(ts_han.end_time)))

# We can directly plot the time series as follows
pylab.plot(ts_han.sample_times, ts_han)
pylab.ylabel('Strain')
pylab.xlabel('Time (s)')
pylab.show()
```

Figure 4.5 Time series data for GW150914

data around specific events also from the full data sets which have been released which cover the S5/S6/O1 LIGO observatories. Data will be returned as pycbc TimeSeries objects.

One can directly retrieve data around a specific event. Typically this data is centered on the event, though restrictions may apply which have not allowed this. This method by default gets the smallest version of the dataset. If additional data or specific versions are required, please see the following two additional ways to access data (for example) shown in figure(4.5).

Figure 4.6Getting Data from S5 / S6 / O1

```
# We'll first download some data for this demonstration
!curl -O -J -L https://losc.ligo.org/s/events/LVT151012/H-H1_LOSC_4_V2-1128678884-32.gwf

% Total    % Received % Xferd  Average Speed   Time     Time      Current
          Dload  Upload Total Spent   Left Speed
100  266  100  266  0     0  310      0 --::-- --::-- --::-- 309
100 1004k 100 1004k 0     0  322k      0 0:00:03 0:00:03 --::-- 576k

from pycbc.frame import read_frame

# Read the data directly from the Gravitational-Wave Frame (GWF) file.
file_name = "H-H1_LOSC_4_V2-1128678884-32.gwf"

# L OSC bulk data typically uses the same convention for internal channels names
# Strain is typically IFO:LOSC-STRAIN, where IFO can be H1/L1/V1.
channel_name = "H1:LOSC-STRAIN"

start = 1128678884
end = start + 32

ts = read_frame(file_name, channel_name, start, end)
```

Figure 4.7Reading-gravitational-wave-frame

4.3.1 Getting Data from S5 / S6 / O1 and Getting Data from S5 / S6 / O1

In this section we show how to read data from the bulk data release by LIGO. This currently covers the periods of teh S5, S6, and O1 analyses and directly read in the data as follows(for example) shown in figure(4.6.4.7).

4.4 Visualization of Data and Signal Processing

In this section we will walk through how to visualize LIGO/Virgo data and how to perform some basic signal processing on it, including high/low passing, psd estimation, and whitening.

4.4.1 Viewing the raw LIGO data

In the figure(4.8) we will view the raw ligo data. You should notice that there is signifiant low frequency content (indicated by the large oscilations) and even some DC offset in the data and plot the corresponding values in the form of the strain along the y axis and the time along the x axis(for

```
%matplotlib inline

# Read in the data around GW150914
from pycbc.catalog import Merger
import pylab

m = Merger('GW150914')

data = {}
for ifo in ['H1', 'L1']:
    data[ifo] = m.strain(ifo)
```

Entire 32 seconds of data round GW150914

```
for ifo in data:
    pylab.plot(data[ifo].sample_times, data[ifo], label=ifo)

pylab.ylabel('Strain')
pylab.xlabel('GPS Time (s)')
pylab.legend()
pylab.show()
```

Figure 4.8 Viewing-the-raw-ligo-data

example consider the gravitational wave GW150914 you just zoom in to one second around, all you can see is the low frequency behavior of the noise, since it is much louder than the higher frequency noise (and signal).

4.4.2 Highpass and power spectral density (PSD) of the data ? and

We apply a highpass filter to the data to suppress the low frequency noise of the instrument. We can see that this brings the dynamic range of the data largely into the same range. However, there is clearly still some dominant frequencies. To equalize this, we would need to apply a whitening filter.

Understanding how the noise power varies over frequency is important for LIGO data analysis. In this section we use a version of Welch's method to estimate the power spectral density of the data. Note that there is a significant amount of noise at low frequencies (orders of magnitude). also that there is a large amount of power at a few specific frequencies. derive the corresponding Highpass method to remove the low frequency

```

for ifo in data:
    # Apply a highpass filter to the data. This suppresses the low
    # frequency content of the data. We choose here a finite-impulse-response (FIR).
    # Options
    # 1) highpass frequency
    # 2) half sample length of highpass filter
    #(higher value will give less ripple in passband)
    high_data = data[ifo].highpass_fir(15, 512) # Highpass point is 15 Hz

    # The time slice method can give just a portion of the time
    # series using GPS start and stop times
    zoom = high_data.time_slice(m.time - 0.5, m.time + 0.5)
    pylab.plot(zoom.sample_times, zoom, label=ifo)

pylab.legend()
pylab.show()

```

Figure 4.9 Applying highpass filter to data

```

for ifo in data:
    # This estimates the PSD by sub-dividing the data into overlapping
    # 4s long segments. (See Welch's method)
    psd = data[ifo].psd(4)

    # Note that the psd is a FrequencySeries!
    pylab.loglog(psd.sample_frequencies, psd)

```

Figure 4.10 PSD

content and to see the power spectral density of data we use the corresponding codes shown in figure(4.9,4.10).

4.4.3 Whitening the data and Visualizing excesses in the data with a Q-transform plot

To visualize deviations from the noise, use `to` "whiten" the data within some frequency range. This way excesses in the data are visible as deviations from zero. Whitening takes the data and attempts to make the power spectral density flat, so that all frequencies contribute equally. We will whiten the data, and then bandpass the result to focus on a specific frequency range. We will now bandpass the data around (for example) GW150914 between 30 - 250 Hz. This will remove frequency ranges which won't contribute to this kind of signal and make it possible to see the signal in question. After doing this there is some excess signal that sticks above the noise. Let's zoom around this time now, and align the two time series. We choose a tighter to a particular time and zoom. Then we get the

```

# Whiten the data
whitened = {}

for ifo in data:
    # This produces a whitened set.
    # This works by estimating the power spectral density from the
    # data and then flattening the frequency response.
    # (1) The first option sets the duration in seconds of each
    #     sample of the data used as part of the PSD estimate.
    # (2) The second option sets the duration of the filter to apply
    whitened[ifo] = data[ifo].whiten(4, 4)

zoom = whitened[ifo].time_slice(m.time - 0.5, m.time + 0.5)
pylab.plot(zoom.sample_times, zoom, label=ifo)

```

Figure 4.11 whitlening the data

```

pylab.figure(figsize=[15, 3])
for ifo in whitened:
    # Apply a highpass filter (at 30 Hz) followed by an lowpass filter (at 250 Hz)
    bpsd = whitened[ifo].highpass_fir(30, 512).lowpass_fir(250, 512)

    # Now we'll specially align the L1 data. Where does this come from?
    # (1) We already knew that the signal was ~ 7 ms separated between detectors.
    # (2) The two LIGO interferometers are roughly aligned so that the output of
    #     one is a sign change of the other for *many* sky locations. This is an
    #     approximation and doesn't hold for all possible source sky locations.
    # A later tutorial will show how to estimate this alignment more precisely.
    if ifo == 'L1':
        bpsd.roll(int(bpsd.sample_rate * .007))
        bpsd *= -1

    # We'll choose a tighter zoom here.
    zoom = bpsd.time_slice(m.time - 0.2, m.time + .1)
    pylab.plot(zoom.sample_times, zoom, label=ifo)

```

Figure 4.12 coherent signal that matches in phase for a few cycles

coherent signal that matches in phase for a few cycles.

A common way to visualize gravitational-wave data is with a time-frequency representation known as the constant-Q transform. This is similar to a standard spectrogram made with short-time Fourier transforms with the advantage that frequency bins are more sparsely spaced at high frequencies. The corresponding codes are shown in the figure (4.11, 4.12, 4.13). The transform can be a powerful diagnostic tool; however, note that quieter signals, especially those with lower masses and will be harder to spot visually. In practice, we use a technique called matched filtering to find signals in our data.

Figure 4.13 Q-transform

```
%matplotlib inline
from pycbc.waveform import get_td_waveform
import pylab

# The output of this function are the "plus" and "cross" polarizations of the gravitational-wave signal
# as viewed from the line of sight at a given source inclination (assumed face-on if not provided)
hp, hc = get_td_waveform(approximant='SEOBNRv4_opt',
                         mass1=10,
                         mass2=10,
                         delta_t=1.0/4096,
                         f_lower=30)
```

Figure 4.14 Generating waveform

4.5 Generating Waveforms and Matched Filtering

Here we'll generate the gravitational waveform using one of the available waveform approximants. These can be generated as a time series using `get_td_waveform`. There are some additional examples using this interface here. The key parameters are the masses of the binary (given in solar masses), the time between samples (in seconds), the starting gravitational-wave frequency (Hz) and the name of the approximant we'd like to generate. A variety of approximants are available that include different physical effects.

We use different models and as well with different methodologies available in the module. Let's consider the example we've chosen to use the `'SEOBNRv4opt'` model. It models the gravitational waveform of inspiralling and merging black holes, and includes the ability for each black hole to spin in the same direction as the orbit (aligned spins). Corresponding code for this simulation shown in the figure(4.14).

We can see that the length of the waveform increases for lower mass binary merger. The distance of the waveform is also selectable when you generate a waveform. The units used are Megaparsecs. Keep in mind that no redshift effects are taken into account here, so there is a simple linear relationship between distance and amplitude.

Looking for a specific signal in the data, then matched filtering is known to be the optimal method in Gaussian noise to extract the signal. When the parameters of the signal are unknown, one can test for each set of parameters one is interesting in finding after this econditioning the data

```

from pycbc.psd import interpolate, inverse_spectrum_truncation
# Estimate the power spectral density

# We use 4 second samles of our time series in Welch method.
psd = conditioned.psd(4)

# Now that we have the psd we need to interpolate it to match our data
# and then limit the filter length of 1 / PSD. After this, we can
# directly use this PSD to filter the data in a controlled manner

psd = interpolate(psd, conditioned.delta_f)

# 1/PSD will now act as a filter with an effective length of 4 seconds
# Since the data has been highpassed above 15 Hz, and will have low values
# below this we need to inform the function to not include frequencies
# below this frequency.
psd = inverse_spectrum_truncation(psd, int(4 * conditioned.sample_rate),
                                    low_frequency_cutoff=15)

```

Figure 4.15 power spectral density

to reduce the dynamic range of the data and suppress low frequency behavior which can introduce numerical artifacts. We may also wish to resample the data if high frequency content is not important.

4.5.1 calculate the power spectral density and signal model

Optimal matched filtering requires weighting the frequency components of the potential signal and data by the noise amplitude. We can view this as filtering the data with the time series equivalent PSD. To ensure that we can control how much applying this filter to the data, we window the time domain equivalent of the PSD to a specific length. This effect of losing some information about line behavior in the detector, since our signal spans a large frequency range, and lines are narrow, this is a negligible effect.

Conceptually, matched filtering involves laying the potential signal over your data and integrating (after weighting frequencies correctly) is a signal in the data that aligns with your 'template', you will get a large value when integrated over which can be done by using the following code shown in the figure(4.15,4.16).

```

# In this case we "know" what the signal parameters are. In a search
# we would grid over the parameters and calculate the SNR time series
# for each one

# We'll assume equal masses, which is within the posterior probability
# of GW150914.
m = 36 # Solar masses
hp, hc = get_td_waveform(approximant="SEOBNRv4_opt",
                         mass1=m,
                         mass2=m,
                         delta_t=conditioned.delta_t,
                         f_lower=20)

# We will resize the vector to match our data
hp.resize(len(conditioned))

```

Figure 4.16signal model

```

# In this case we "know" what the signal parameters are. In a search
# we would grid over the parameters and calculate the SNR time series
# for each one

# We'll assume equal masses, which is within the posterior probability
# of GW150914.
m = 36 # Solar masses
hp, hc = get_td_waveform(approximant="SEOBNRv4_opt",
                         mass1=m,
                         mass2=m,
                         delta_t=conditioned.delta_t,
                         f_lower=20)

# We will resize the vector to match our data
hp.resize(len(conditioned))

```

Figure 4.17Aligning and Subtracting the Proposed Signal

4.6 signal-to-noise time series

In this section we will now calculate the signal-to-noise time series for our template. We'll take care to handle issues of filter corruption / wraparound by truncating the output time series. We need to account for both the length of the template and the SNR . We can use this SNR peak to align our proposal to the data, and to also subtract our proposal from the data and Aligning and Subtracting the Proposed Signals, which can done using the following code figure(4.17).

4.7 Subtracting the signal from the data

To compare the data and signal on equal footing, and to concentrate on the frequency range that is important, we will whiten both the template and the data, and then bandpass both the data and template between 30-300

```

subtracted = conditioned - aligned

# Plot the original data and the subtracted signal data

for data, title in [(conditioned, 'Original H1 Data'),
                     (subtracted, 'Signal Subtracted from H1 Data')]:
    t, f, p = data.whiten(4, 4).qtransform(.001,
                                           logfsteps=100,
                                           qrange=(8, 8),
                                           frange=(20, 512))

```

Figure 4.18 Subtracting the signal from the data

Hz. In this way, any signal that is in the data is transformed in the same way as the template. Now that we've aligned the template we can simply subtract it. Let's see below how that looks in the time-frequency plots. Which can done by shown in the figure (4.18).

4.8 Results and conclusions

4.8.1 mergers name in catalog

- GW170823-v1
- GW170818-v1
- GW170817-v3
- GW170814-v3
- GW170809-v1
- GW170729-v1
- GW170608-v3
- GW170104-v2
- GW151226-v2
- GW151012-v3
- GW150914-v3

Parameters of GW150914

Chirp Mass of GW150914 Source Frame: 2.6e6 Solar Masses Detector Frame:

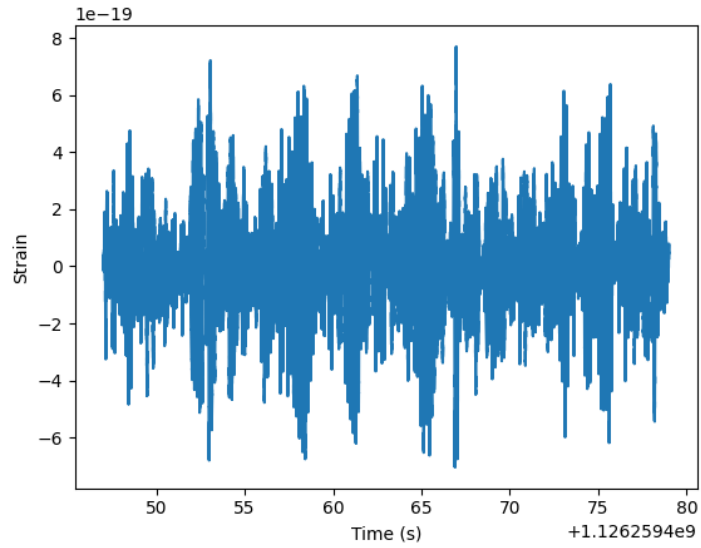


Figure 4.19 Duration:32.0s Start:1126259447 End:1126259479

% Total	% Received	% Xferd	Average Speed	Time	Time	Time	Current
Dload	Upload	Total	Spent	Left	Speed		
100	253	100	253	0	642	0	643
100	1004k	100	1004k	0	910k	0:00:01	2608k

Figure 4.20 Data for this demonstration

31.174000000000003 Solar Masses Returned 64.0s of data at 4096.0Hz

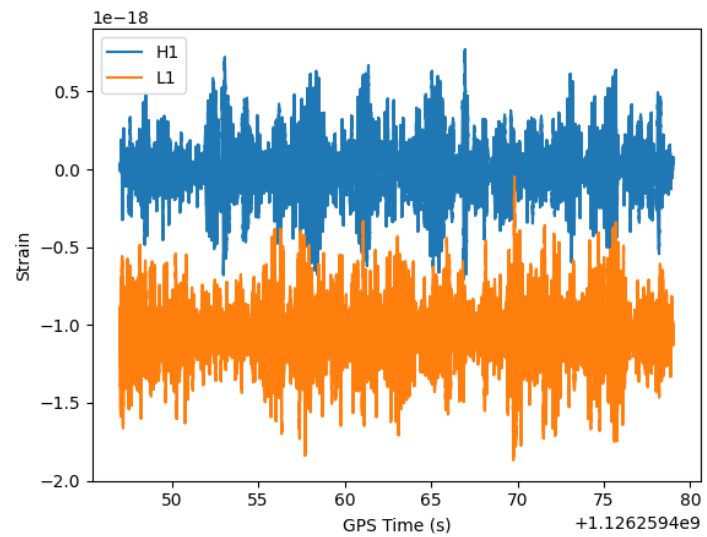


Figure 4.21'H1', 'L1'

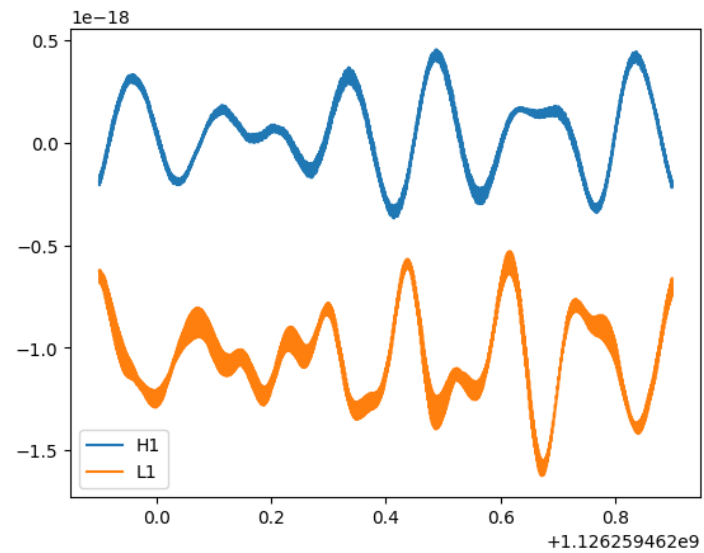


Figure 4.22Zoomed to 0.5s

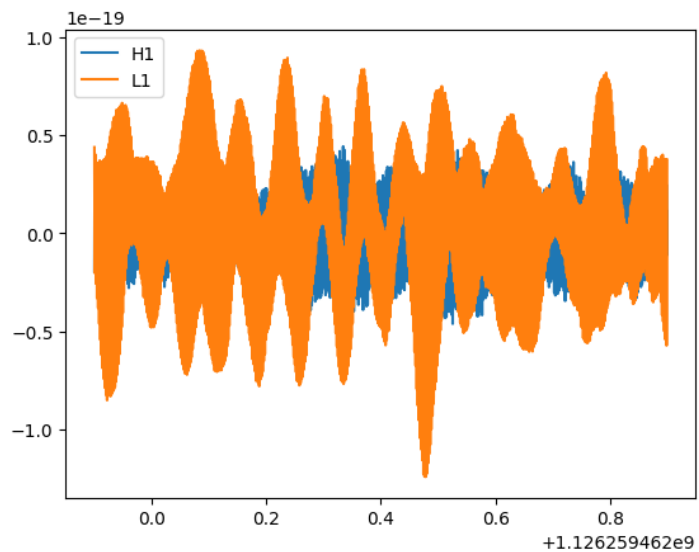


Figure 4.23 highpass frequency

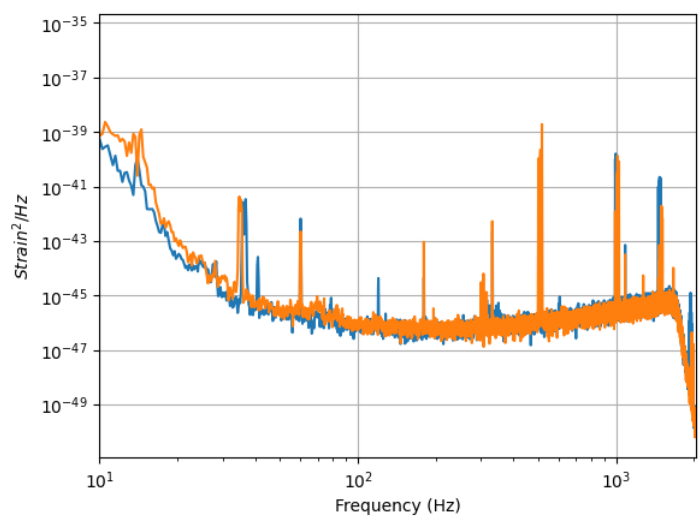


Figure 4.24 psd is a FrequencySeries

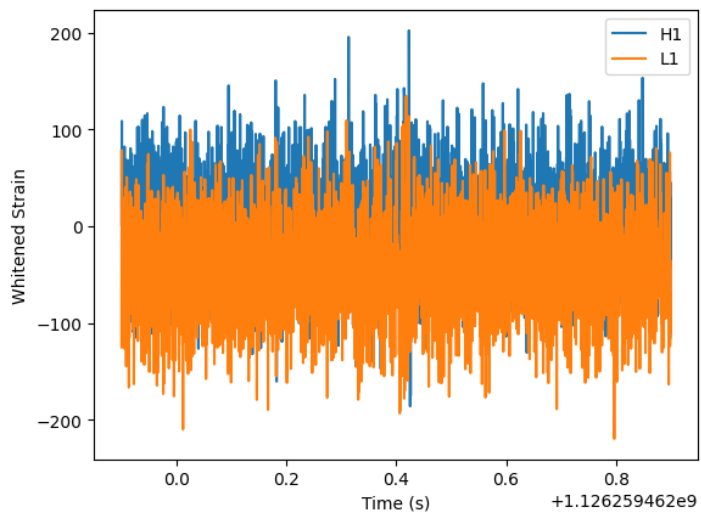


Figure 4.25Whiten the data

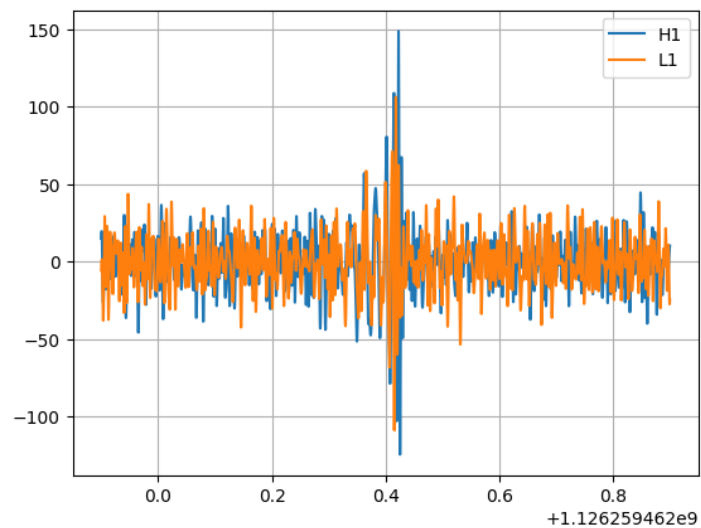


Figure 4.26Apply a highpass filter (at 30 Hz) followed by an lowpass filter (at 250 Hz)

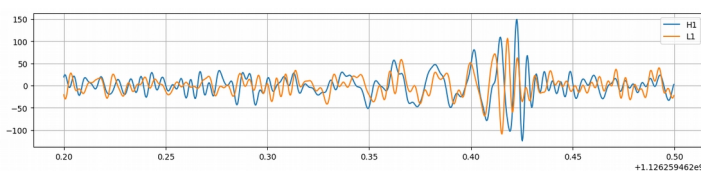


Figure 4.27Apply a highpass filter (at 30 Hz) followed by an lowpass filter (at 250 Hz) to tighter

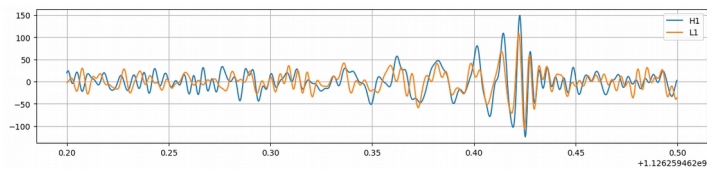


Figure 4.28specially align the L1 data

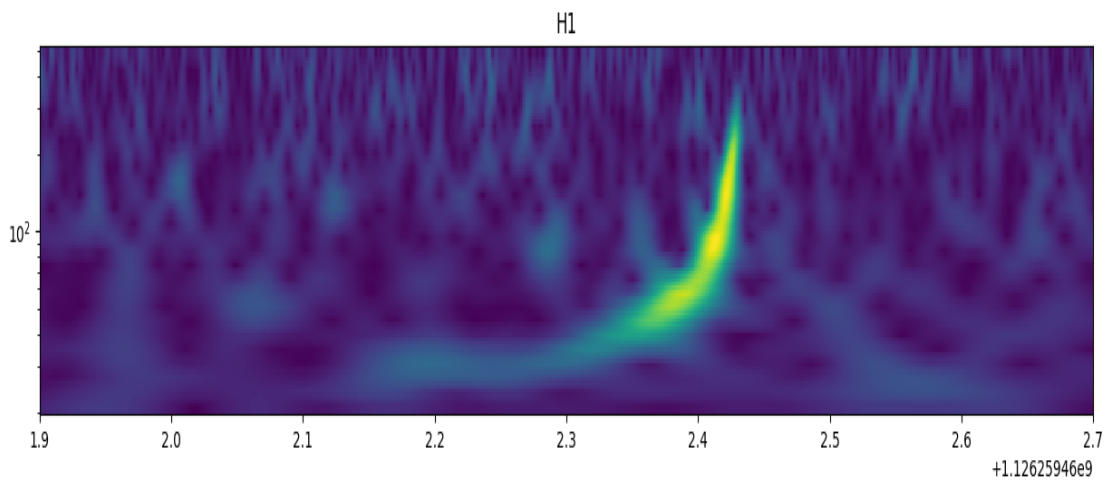


Figure 4.29visualizing excesses in the data with a Q-transform plot

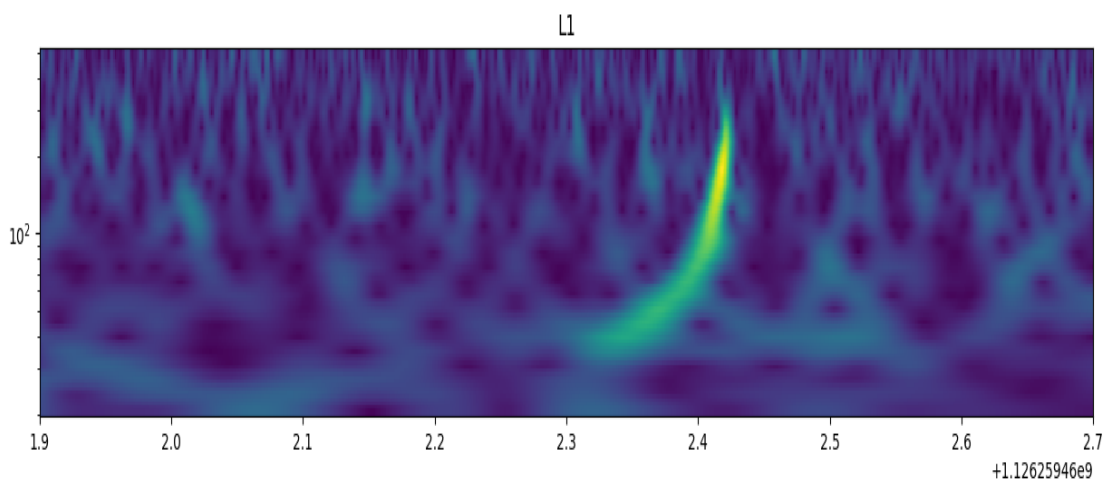


Figure 4.30visualizing excesses in the data with a Q-transform plot

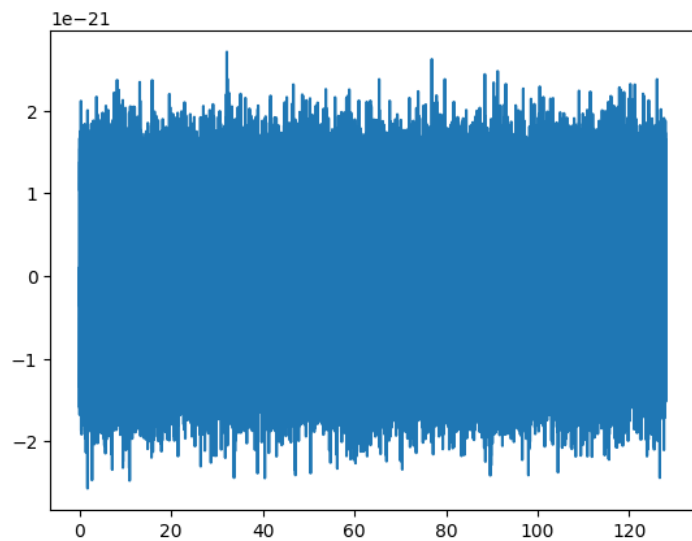


Figure 4.31 TEST-STRAIN

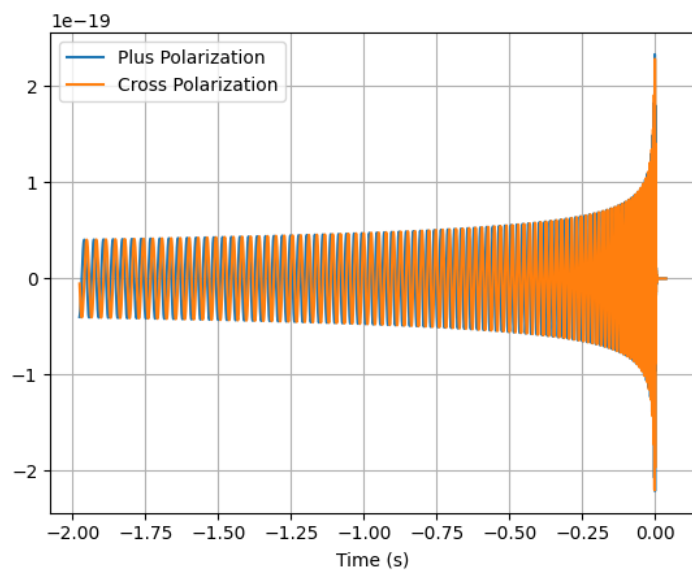


Figure 4.32 Generating waveform

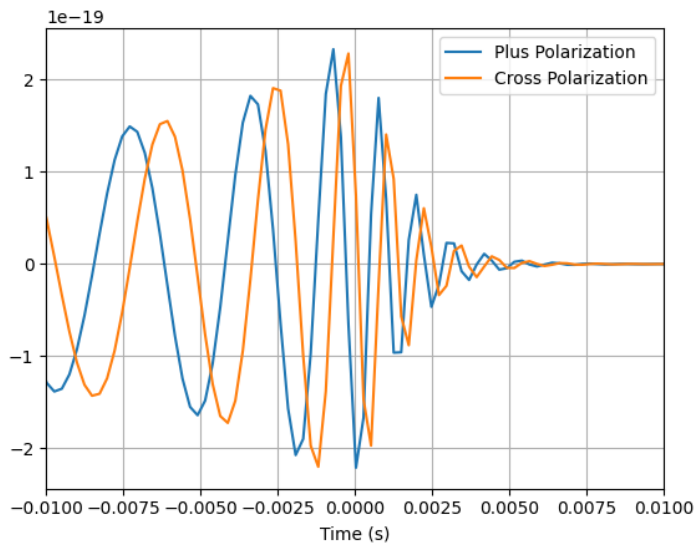


Figure 4.33 Waveform zoomed to 0.01s

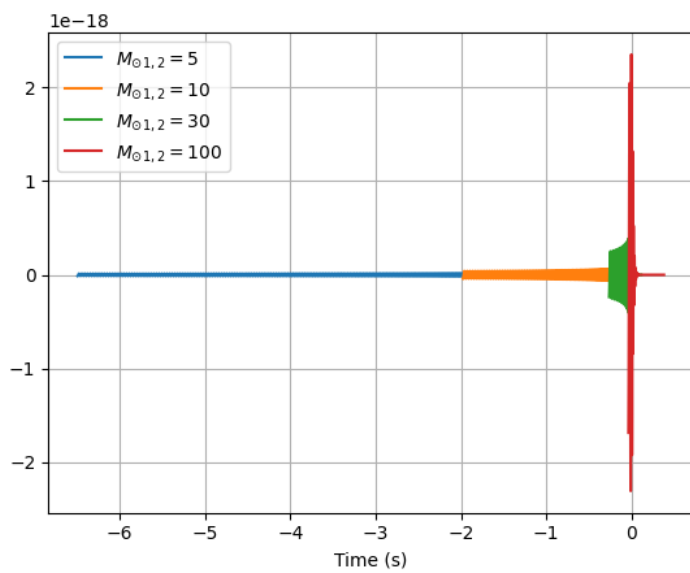


Figure 4.34 Waveform change with the mass of the binary

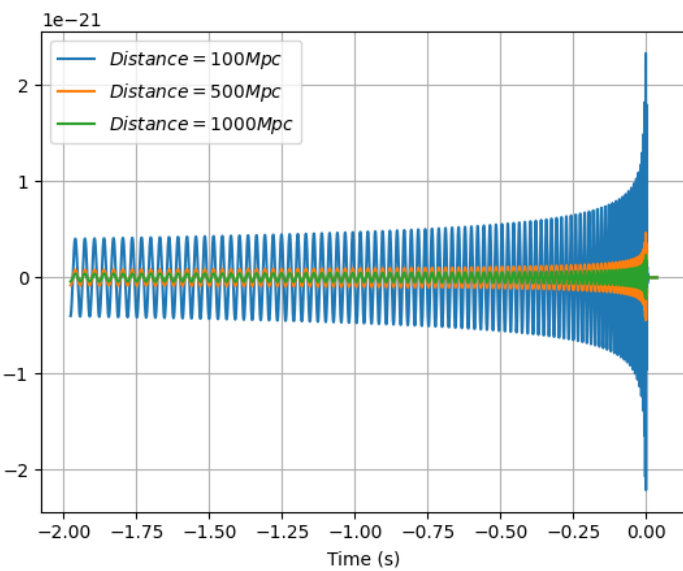


Figure 4.35 Changing the distance of the waveform

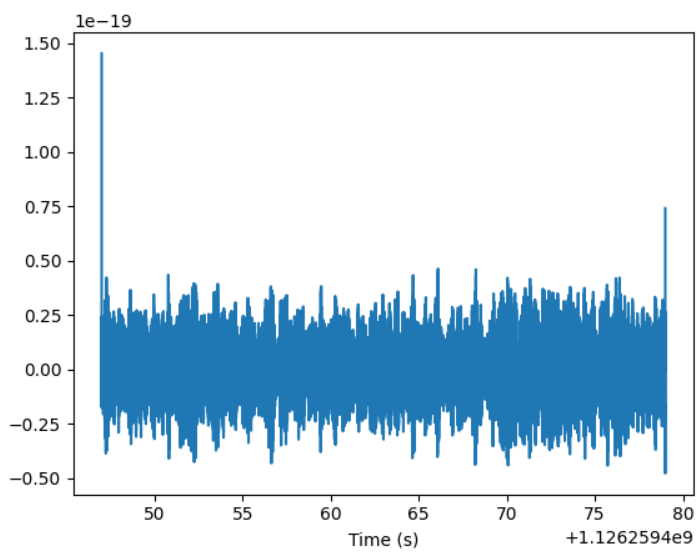


Figure 4.36 Remove the low frequency content and downsample the data to 2048Hz

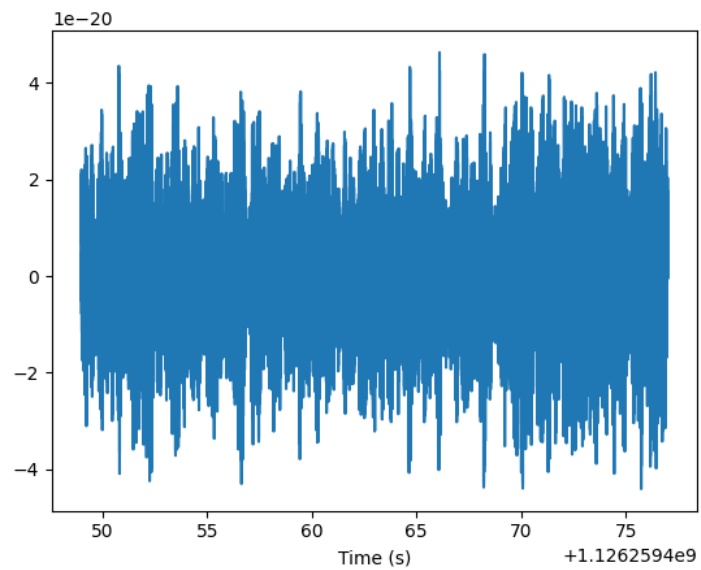


Figure 4.37 Remove 2 seconds of data from both the beginning and end

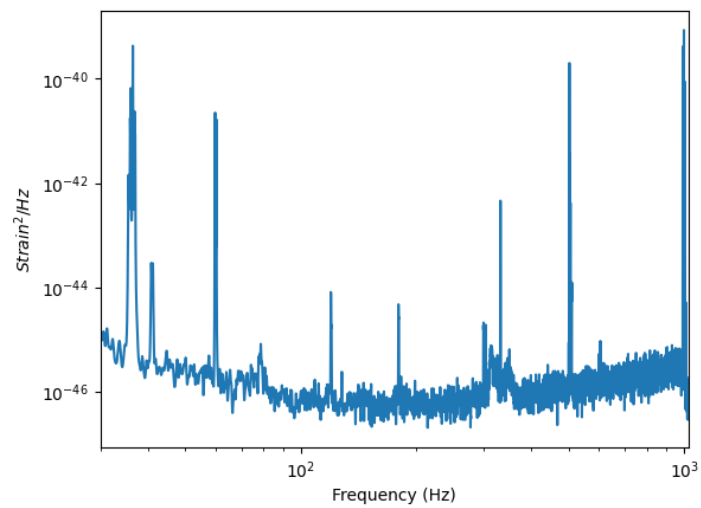


Figure 4.38 Power spectral density

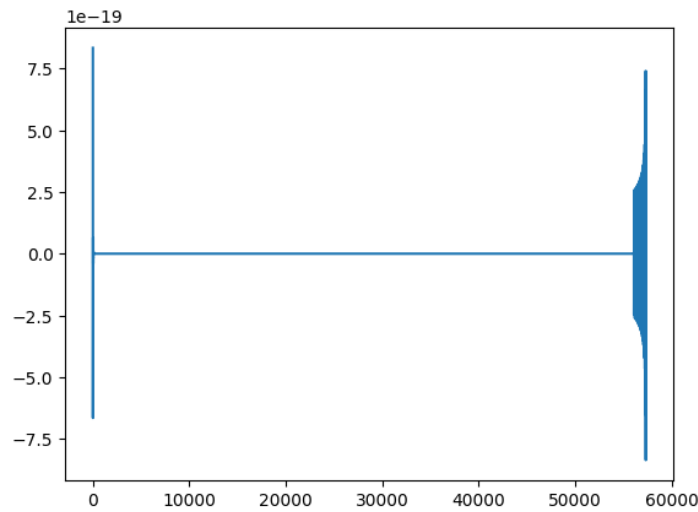


Figure 4.39 Our signal model and matched filtering involves laying the potential signal over our data and integrating

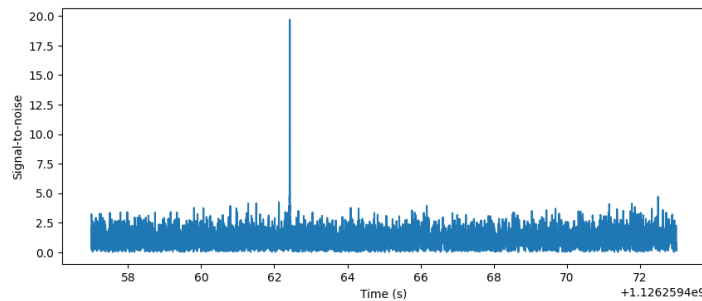


Figure 4.40 Calculating the signal-to-noise time series

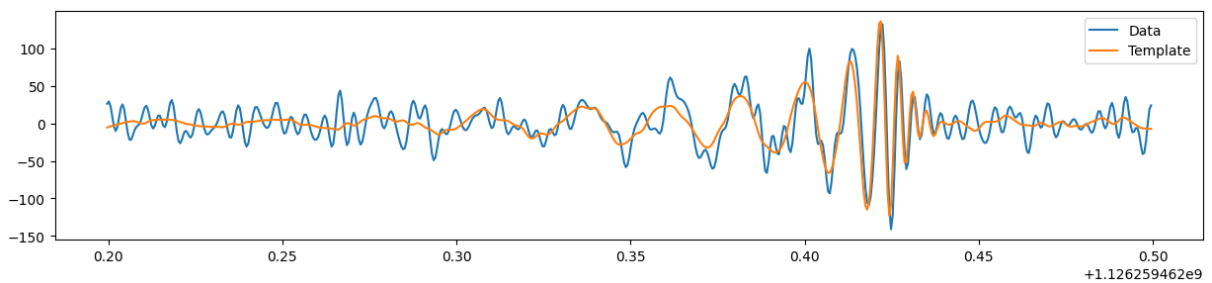


Figure 4.41 Visualize the overlap between the signal and data

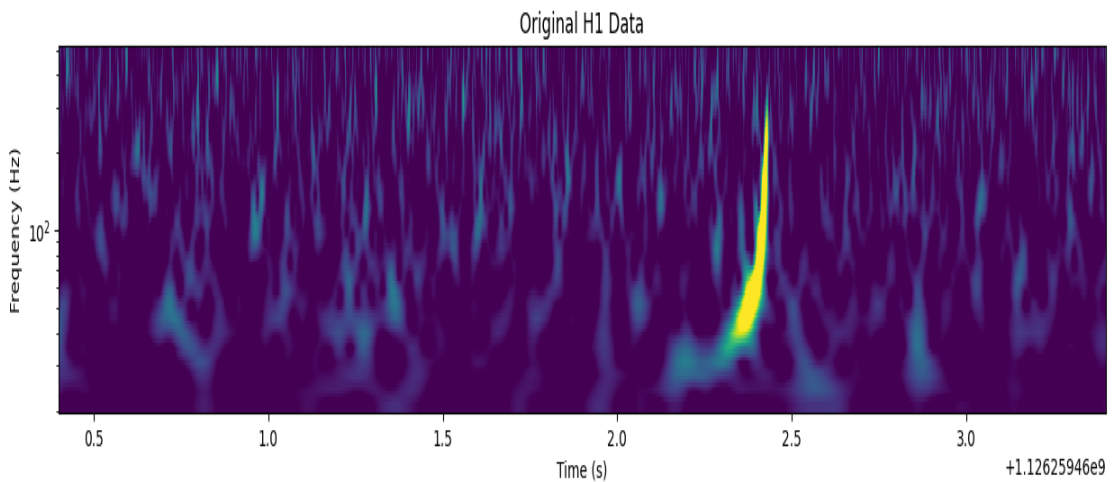


Figure 4.42 Subtracting the signal from the data

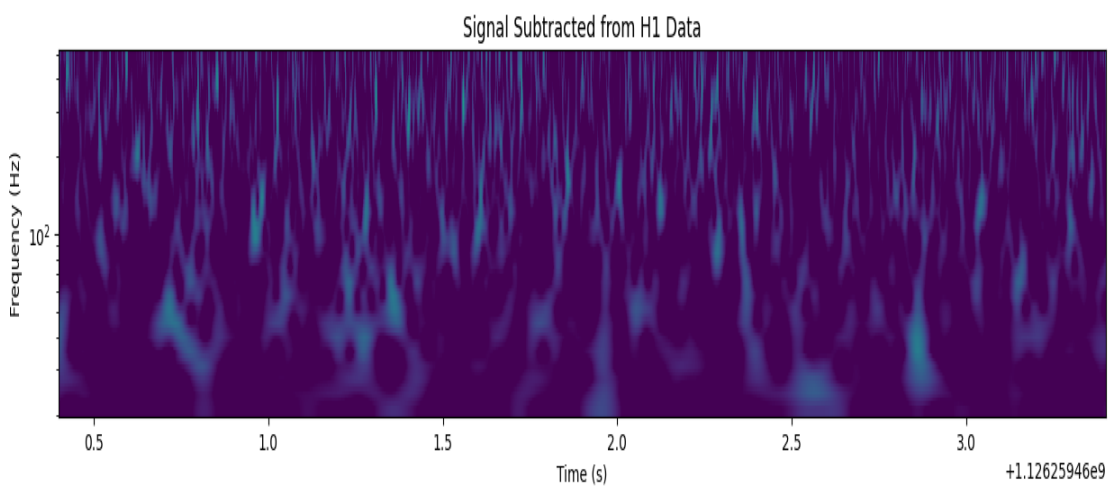


Figure 4.43 Subtracting the signal from the data